"Cloud Slicing": A new technique to derive tropospheric ozone profile information from satellite measurements

J. R. Ziemke[1]
SGT, Greenbelt, Maryland

S. Chandra and P. K. Bhartia
NASA Goddard Space Flight Center, Greenbelt, Maryland

Submitted to *Journal of Geophysical Research*, August 28, 2000.

[1]Also at NASA Goddard Space Flight Center, Greenbelt, Maryland.

Abstract. A new technique denoted cloud slicing has been developed for estimating tropospheric O_3 profile information. All previous methods using satellite data were only capable of estimating the total column of O_3 in the troposphere. Cloud slicing takes advantage of the opaque property of water vapor clouds to ultraviolet wavelength radiation. Measurements of above-cloud column O_3 from the Nimbus 7 total ozone mapping spectrometer (TOMS) instrument are combined together with Nimbus 7 temperature humidity and infrared radiometer (THIR) cloud-top pressure data to derive O_3 column amounts in the upper troposphere. In this study tropical TOMS and THIR data for the period 1979-1984 are analyzed. By combining total tropospheric column ozone (denoted TCO) measurements from the convective cloud differential (CCD) method with 100-400 hPa upper tropospheric column O_3 amounts from cloud slicing, it is possible to estimate 400-1000 hPa lower tropospheric column O_3 and evaluate its spatial and temporal variability. Results for both the upper and lower tropical troposphere show a year-round zonal wavenumber 1 pattern in column O_3 with largest amounts in the Atlantic region (up to ~15 DU in the 100-400 hPa pressure band and ~25-30 DU in the 400-1000 hPa pressure band). Upper tropospheric O_3 derived from cloud slicing shows maximum column amounts in the Atlantic region in the June-August and September-November seasons which is similar to the seasonal variability of CCD derived TCO in the region. For the lower troposphere, largest column amounts occur in the September-November season over Brazil in South America and also southern Africa. Localized increases in the tropics in lower tropospheric O_3 are found over the northern region of South America around August and off the west coast of equatorial Africa in the March-May season. Time series analysis for several regions in South America and Africa show an anomalous increase in O_3 in the lower troposphere around the month of March which is not observed in the upper troposphere. The eastern Pacific indicates weak seasonal variability of upper, lower, and total tropospheric O_3 compared to the western Pacific which shows largest TCO amounts in both hemispheres around spring

months. O_3 variability in the western Pacific is expected to have greater variability caused by strong convection, pollution and biomass burning, land/sea contrast and monsoon developments.

1. Introduction

The determination of tropospheric ozone (O_3) from satellite retrievals has a growing history beginning with *Fishman et al.* [1990]. In that study a residual method was used where the total column of tropospheric ozone (hereafter denoted tropospheric column ozone, TCO) was derived by subtracting stratospheric column ozone (SCO) (via Stratospheric Aerosols and Gas Experiment, SAGE) from total column ozone (via total ozone mapping spectrometer, TOMS). Because of the sparse temporal and spatial coverage of SAGE data, the derived fields of SCO and TCO were best suited for studying seasonal cycle climatologies. *Fishman et al.* [1996] and *Vukovich et al.* [1996] estimated daily fields of TCO. Both of these investigations used Solar Backscatter Ultraviolet (SBUV) O_3 measurements to derive SCO. In the study by *Vukovich et al.* [1996] extensive comparisons were made with ground based measurements and significant discrepancies were noted. Because of the nature of the SBUV retrieval algorithm, O_3 disturbances in the troposphere propagate into the SCO fields, producing noise and data artifacts in determined residual fields of TCO. A new and improved approach to using SBUV data for deriving SCO and TCO was shown by *Fishman and Balok* [1999] in which SBUV data were adjusted using ozonesonde data. The method proved useful for determining daily regional maps of TCO outside the tropics for tracking pollution events.

Hudson and Thompson [1998] proposed a modified residual method for the tropics which combined TOMS and ozonesonde measurements. Their method assumes that the longitudinal variation of total column O_3 at the equator consists of an underlying wavenumber 1 structure with superimposed smaller scale fluctuations which they characterize as "excess ozone" and attribute primarily to biomass burning. The wavenumber 1 structure is assumed to consist of a zonally invariant stratospheric component and a tropospheric component consisting of a constant background and a zonally varying wavenumber 1 component. The latter is determined by fitting a sinusoid

to total column O_3 using only Pacific data which is then subtracted from the total column O_3 to estimate "excess ozone". Unfortunately the non-fluctuating component of tropospheric O_3 cannot be uniquely determined from TOMS measurements alone and must be evaluated using another set of O_3 measurements. However, it needs to be evaluated at only one longitude to calculate SCO which is assumed to be zonally invariant. *Hudson and Thompson* [1998] used ozonesonde data from a number of stations in the Atlantic region and concluded that for the 1991-1992 time period, the non-fluctuating component of tropospheric O_3 in this region had a mean value of about 24 DU with an additional seasonal variability of around 5 DU amplitude. They further assumed that these values do not change from year to year. The modified residual method may thus not fully account for the interannual variability of tropospheric O_3 which is driven largely by El Niño and La Niña events in the Pacific [*Chandra et al.*, 1998]. The data may be best suited for the Atlantic region [*Thompson and Hudson*, 1999].

Ziemke et al. [1998] introduced two new methods for deriving TCO in the tropics. The first was to use assimilated microwave limb sounder (MLS) and halogen occultation experiment (HALOE) SCO measurements to derive TCO. This was a residual method similar to *Fishman et al.* [1990] and used TOMS measurements of total column O_3. The advantage with this approach is that daily maps of high spatial coverage can be obtained. The main limitation of this approach was the combination of two stratospheric instrument measurements with TOMS total O_3, resulting in sizable inter-instrument calibration errors in calculated TCO. The second approach for deriving TCO by *Ziemke et al.* [1998] used optically thick convective clouds, hence denoted the convective cloud differential (CCD) method. This second method was limited to the tropics because it required persistent high reflectivity tropopause-level clouds to develop month to month gridded time series. In the CCD method total column ozone is derived from low reflectivity ($R < 0.2$) measurements and SCO follows from nearby

column ozone measurements taken above the tops of very high tropopause-level clouds under conditions of high reflectivity ($R > 0.9$). First, above-cloud column amounts are calculated in the Pacific region where tropopause-level clouds are persistent. SCO is then derived for every 5° latitude band and averaged from 120°E eastward to 120°W using only lowest values of above-cloud column amounts (the lowest values coincide with tropopause-level cloud tops). These SCO values are then assumed to be independent of longitude in a given latitude band. This assumption is based on the characteristics of zonal symmetry of tropical SCO as inferred from Upper Atmosphere Research Satellite (UARS) microwave limb sounder (MLS) and halogen occultation experiment (HALOE) ozone data. We refer the reader to *Ziemke et al.* [1998] for further details regarding the CCD technique. A unique property of the CCD method for deriving TCO is that it is not affected by inter-instrument calibration errors because it only uses TOMS measurements. For the CCD TCO data used in this study several corrections were made including adjustments for sea glint, tropospheric aerosols, and lower tropospheric retrieval inefficiency. These data corrections are discussed in detail in the Appendix.

All of the previous methods using satellite data could only provide estimates of the total column of O_3 in the troposphere. The present study uses a new technique denoted cloud slicing to derive tropospheric O_3 profile information in the tropics from satellite measurements. Cloud slicing in this investigation will be shown to be capable of providing time series of upper and lower tropospheric column O_3 from satellite retrievals when combined with TCO measurements.

2. Overview of Cloud Slicing

The cloud-slicing method for obtaining O_3 profile information is an extension of the CCD technique of *Ziemke et al.* [1998] which derives TCO abundances. A main difference between the two methods is that the CCD technique does not require measurements of cloud-top pressures. Instead, high reflectivity $R > 0.9$ scenes are

incorporated in the tropics providing a data base of tropopause-level cloud tops. While knowledge of cloud-top pressures is not required with the CCD technique, there are several sizable algorithm errors requiring correction for the $R < 0.2$ near clear-sky scenes. These errors have been corrected in the current CCD data and are discussed in the Appendix.

The technique used behind cloud-slicing is shown in the Figure 1 schematic. With this method, co-located measurements of above-cloud column O_3 and cloud-top pressure are combined to yield tropospheric O_3 profile information. Given a database of these two co-located measurements, the derivation of O_3 profile information is then straightforward. Column O_3 ($\Delta\Omega$) between two pressure surfaces P_{low} and P_{high} ($P_{low} < P_{high}$) can be derived by integrating O_3 volume mixing ratio (X) over pressure from P_{low} to P_{high}:

$$\Delta\Omega = 0.788 \cdot \int_{P_{low}}^{P_{high}} dP \cdot X \tag{1}$$

where the units for $\Delta\Omega$, P, and X are Dobson units (DU), hPa, and ppmv, respectively.

From (1) a mean volume mixing ratio (in ppmv) for O_3 in this same pressure interval is given by

$$\overline{X} = 1.27 \cdot \frac{\Delta\Omega}{\Delta P} \tag{2}$$

Figure 1 illustrates high-resolution cloud slicing where satellite FOV footprint measurements are small enough to provide cloud slicing analysis of individual clouds. TOMS measurements however have a large FOV footprint (around 100 km on average) which is often larger than the clouds being used for cloud slicing. The result is often not enough clouds and too much clear-sky in the FOV measurements.

This pilot study of cloud slicing uses a statistical ensemble approach (see Figure 2 schematic) for deriving tropical O_3 VMR by combining many co-located measurements of cloud-top pressure and above-cloud column O_3 over a broad region (5° × 5° bins). This analysis was carried out for monthly averages, and to reduce the number of partially

cloudy footprint scenes only TOMS O_3 measurements with reflectivity R greater than 0.6 were used in the cloud slicing analyses. Scenes with $R > 0.6$ coincide with 100% cloud fraction [*Eck et al.*, 1987] and generally middle to upper tropospheric cloud tops [*Stowe et al.*, 1989]. Once mean VMR is derived, column O_3 follows by inverting (2) to solve for $\Delta\Omega$. The $R > 0.6$ filtering not only reduces the amount of clear-sky contamination but also reduces or eliminates problems such as efficiency factor, sea glint, and tropospheric aerosols that can all seriously affect cloud-slicing measurements.

This study combines co-located measurements of Nimbus 7 temperature humidity infrared radiometer (THIR) cloud-top pressure and Nimbus 7 TOMS column O_3 for the time period 1979-1984. The Nimbus 7 THIR instrument [*Stowe et al.*, 1988] is a two-channel scanning radiometer measuring Earth radiation from two spectral bands, 10.5 to 12.5 μm (11.5 μm mean) and 6.5 to 7.0 μm (6.7 μm mean). The 6.7 μm band provides measurements of moisture in the middle and upper troposphere, and the 11.5 μm band provides cloud-top temperatures. Cloud-top pressures were derived from THIR cloud-top temperatures using a pressure-temperature climatology from National Centers for Environmental Prediction (NCEP). Further details regarding THIR data are discussed by *Stowe et al.* [1988]. The 2σ accuracy of THIR cloud-top pressure footprint measurements used in this study was previously estimated by *Joiner and Bhartia* [1995] to be around 200 hPa. All data in this study were binned to equivalent 5° latitude by 5° longitude block structures centered at latitudes 12.5°S, 7.5°s, ..., 12.5°N, and longitudes 177.5°W, 172.5°W, ..., 177.5°E.

Because of a small number of $R > 0.6$ cloud tops in the lower troposphere, our study derives gridded time series of mean upper tropospheric VMR (and corresponding O_3 column) in the 100 hPa to 400 hPa pressure band. Figure 3 shows the average number of co-located footprint measurements per month of TOMS above-cloud column O_3 and THIR cloud-top pressure in the 100-400 hPa interval over the 1979-1984 time period. Highest numbers (greater than 150) of co-located measurements lie in the

western Pacific, with similar high numbers (~100) over western South America, western Africa, and the north Atlantic. In this study the minimum number of co-located data pairs for any given month within any 5° × 5°bin was taken to be 30 in order to provide adequate statistics for developing monthly time series and seasonal cycle climatologies. Regions such as the south Atlantic and south Pacific west of South America on average have less than 20 data pairs per month.

3. Statistical Ensemble Scatter Diagrams

Figure 4 shows monthly scatter plots of TOMS $R > 0.6$ above-cloud column O_3 versus THIR cloud-top pressure for February 1981 at 2.5°N in the Atlantic region (top three frames) and western Pacific region (bottom three frames). Line fits were applied in each case to all data pairs shown with derived mean O_3 VMR indicated. Each case in Figure 4 indicates a general linear relationship with significantly larger amounts of mean O_3 VMR in the Atlantic than in the Pacific.

4. Horizontal Distributions of Tropospheric O_3

Figure 5 shows zonal variations of CCD TCO (top curves), 400-1000 hPa column O_3 (middle curves), and 100-400 hPa column O_3 (bottom curves) at latitude 2.5°N (Figure 5a) and 2.5°S (Figure 5b). These line plots are based on a 6-year (1979-1984) climatology and are meant to illustrate zonal and seasonal characteristics. The 400-1000 hPa column O_3 amounts were derived by subtracting 100-400 hPa column O_3 from TCO. Within statistical uncertainties, all three column measurements show a zonal wavenumber 1 pattern year round with largest O_3 amounts in the Atlantic region. Most of the wavenumber 1 pattern originates in the lower troposphere as was indicated previously by *Ziemke and Chandra* [1998] from tropical ozonesonde measurements. The wavenumber 1 distribution in Figure 5 at 2.5°N and 2.5°S is also present at other tropical latitudes as shown by the contour plots of Plates 1-3 for 100-400 hPa column

O_3, TCO, and 400-1000 hPa column O_3, respectively.

There are several regions in Plate 1 such as the south Atlantic and south Pacific west of Peru which do not have data because there are not enough clouds in the upper troposphere to provide reliable estimates of O_3 from ensemble cloud slicing (see Figure 3). Present each season in Plate 1 is a dominant zonal wavenumber 1 pattern with largest O_3 amounts in the Atlantic. The wavenumber 1 pattern in TCO (e.g., Plate 2) was first identified by *Fishman et al.* [1990] by subtracting SAGE SCO from TOMS total column O_3. In Plate 1 the persistent wavenumber 1 pattern in 100-400 hPa column O_3 is largest in June-August and September-November seasons, similar to the seasonal behavior in Plate 2 for TCO.

Regional patterns and seasonal cycles in lower tropospheric column O_3 are shown in Plate 3 and were derived by subtracting column amounts in Plate 1 from column amounts in Plate 2. The horizontal patterns in lower tropospheric column O_3 in Plate 3 show a ubiquitous zonal wavenumber 1 pattern with largest column amounts in the September-November season over Brazil in South America and southern Africa. There also appears to be regional increases over the northern region of South America in June-August and off the west coast of equatorial Africa in the March-May season.

5. Time Series and Seasonal Cycles

Time series for the region off the west coast of equatorial Africa are illustrated in Figure 6. For better visualization of seasonal and interannual variabilities the time series for 100-400 hPa column O_3 were also digitally low-pass filtered (shown in bold) with half-frequency response at 5 months. The climatologies (bottom two frames) indicate within statistical uncertainties that the relative increase in northern spring season TCO may be the result of lower tropospheric O_3, since upper tropospheric column O_3 from cloud slicing shows no such increase. A relative increase in lower tropospheric column O_3 may also be present in August-October months.

Figure 7 shows time series over western Brazil in South America where there is a more persistent seasonal cycle in TCO. The upper frames in Figure 7 show large increases in TCO around September months and secondary maxima around March each year. Upper tropospheric column O_3 (bottom curves) indicate large increases around September each year but no increase in March. As the lower two frames in Figure 7 imply, the March increase in TCO within statistical uncertainties may be attributed to increases in lower tropospheric O_3. A similar conclusion was noted for Figure 6 for the region west of equatorial Africa.

For the northern region of South America, a similar seasonal cycle pattern appears in TCO as shown in Figure 8. Largest TCO amounts occur during August-September months with a secondary maximum in March. The upper and lower tropospheric column O_3 climatology series in Figure 8 imply that the increase in March likely comes from the lower troposphere.

Seasonal cycles in tropospheric O_3 over the Pacific Ocean provide insight to the impact of differing land/ocean convection systems and topographic influence. Figures 9 and 10 show seasonal cycles in tropospheric column O_3 over the western Pacific (Figure 9) and eastern Pacific (Figure 10). In Figure 9 over the western Pacific where there is influence from land/ocean contrast and seasonal monsoon developments, there are strong seasonal cycles present between hemispheres. Largest TCO abundances appear around spring months in both hemispheres. Upper and lower tropospheric column O_3 within statistical uncertainties show similar seasonal cycles.

Figure 10 illustrates seasonal variabilities over a broad zonal region in the eastern Pacific at 7.5°N. This latitude was chosen as an example because of a large amount of clouds present for developing time series from cloud slicing (see Figure 3). Upper, lower, and total column O_3 measurements all appear to have weak seasonal variability over the eastern Pacific. Weak seasonal variability was indicated by *Ziemke et al.* [1998] in CCD derived TCO throughout the eastern Pacific and ozonesonde measurements from Samoa

(14°S, 170°W).

Validation of column O_3 amounts from cloud slicing include comparison with ozonesonde measurements. For the 1979-1984 time period, only ozonesonde data from Natal (5°S, 35°W) exist in the tropics to compare with cloud slicing column amounts. Figure 11 shows Natal ozonesonde and cloud slicing column O_3 amounts centered at grid point 2.5°S, 32.5°W. Because of the dry season in Brazil, several months of data from cloud slicing in Figure 11 are missing because there are too few clouds present for reliable cloud slicing results.

6. Summary

Cloud slicing as presented in this study is the first to distinguish between upper and lower tropospheric O_3 from satellite measurements. All previous methods using satellite data could only estimate the total column of O_3 in the troposphere. Co-located measurements of above-cloud column O_3 from the TOMS instrument were combined with THIR cloud-top pressure data on the Nimbus 7 satellite platform for the period 1979-1984 to derive O_3 abundances in the upper troposphere. Using a residual subtraction method with 100-400 hPa upper tropospheric column O_3 from cloud slicing and CCD derived TCO, it was possible to estimate column O_3 in the lower troposphere (400-1000 hPa) and study its temporal and spatial variabilities.

The analyses indicate a persistent zonal wavenumber 1 pattern for both lower and upper tropospheric column O_3 with largest amounts in the Atlantic region with $\sim$15 DU in the 100-400 hPa pressure band and $\sim$25-30 DU in the 400-1000 hPa pressure band. Column O_3 derived from cloud slicing in the 100-400 hPa pressure band shows largest column amounts in the Atlantic region in the June-August and September-November seasons. This seasonal variability is similar to the seasonal variability of TCO in the region. For the lower troposphere, largest column amounts occur around September-November over Brazil and southern Africa. Regional increases

in lower tropospheric O_3 appear over the northern region of South America centered around August. Increases were also indicated off the west coast of equatorial Africa in the March-May season.

Several regions in South America and Africa indicate increases in O_3 in the lower troposphere around March. This increase in March was not seen in upper tropospheric column O_3 from cloud slicing. In the eastern Pacific there is weak seasonal variability of upper, lower, and total tropospheric column O_3 compared to the western Pacific. In the western Pacific, largest TCO amounts occur around spring months in both hemispheres. In the western Pacific, O_3 variability may be affected by strong convection, pollution and biomass burning, land/sea contrast and associated seasonal monsoon developments.

The present study has shown the feasibility of using cloud slicing to obtain meaningful tropospheric O_3 profile information from satellite measurements. For Nimbus 7 TOMS the FOV footprints are large which hinders results from cloud slicing. Future satellite platforms will have significantly smaller footprint sizes and also improved cloud-top pressure measurements, including the rotational Raman scattering Ring effect [*Joiner and Bhartia*, 1995; *Joiner et al.*, 1995].

Appendix

Corrections Made to CCD Derived TCO

TOMS measurements have several sizable intrinsic errors that should be corrected when deriving TCO. Listed below are three primary corrections made to tropical CCD derived TCO data. The validation of the CCD data is discussed by *Ziemke et al.* [1998] and further by *Ziemke and Chandra* [1999]. These previous studies compared the CCD data with ozonesonde and satellite measurements from Upper Atmosphere Research Satellite (UARS) microwave limb sounder (MLS) and halogen occultation experiment (HALOE).

(1) Aerosols:

Absorbing aerosols (mostly dust and smoke) in the troposphere absorb backscattered UV radiance measured by TOMS, and as a result TOMS underdetermines the true total column O_3 content. An aerosol adjustment was made using the linear technique established by *Torres and Bhartia* [1999]. With this method, adjustments ($\Delta\Omega$) made to total column ozone Ω are given by $\Delta\Omega = 0.01K\Omega I$, where I is the TOMS aerosol index and K is a constant equal to 1.12 for Nimbus 7 and 1.2 for Earth Probe. The aerosol adjustment is generally a few DU, however large adjustments exceeding +10 DU can occur because of optically thick desert dust or smoke coming from intense wildfires. The largest adjustments in TOMS monthly data lie over northern Africa (from both desert dust and smoke from biomass burning) with changes of around +8 DU, and along the west coast of central Africa (smoke from biomass burning) with values around +6 DU.

(2) Sea Glint:

The aerosol adjustment applied to the CCD monthly data also partially corrects for sea glint errors over ocean (Zia Ahmad and Omar Torres, personal communication, 2000). The sea glint effect is a function of solar declination and it is caused by bright surface reflection. For a scene affected by clear-sky sea glint, TOMS underdetermines the true total column O_3 content. Sea glint can cause errors of around -5 to -10 DU in daily measurements and around -1 to -3 DU in monthly means.

(3) Retrieval Efficiency:

Due to strong Rayleigh scattering at UV wavelengths, the TOMS instrument has reduced sensitivity to O_3 in the lower troposphere below about 5 km altitude [e.g., *Klenk et al.*, 1982; *Hudson et al.*, 1995]. Although the TOMS algorithm includes a lower tropospheric efficiency correction, it is based on a climatology. Hence, values of column O_3 greater than or smaller than a certain number (around 35 DU in TCO) require adjustment. For the CCD derived TCO monthly data,

a first-order efficiency correction was applied. In effort to provide an efficiency correction there must first be a clear functional relationship identified between lower tropospheric O_3 and TCO. This relationship to first order is a straight line. Figure 12 is a plot of 0-5 km column O_3 (Ω_{0-5km}) versus TCO (Ω_{TCO}) derived from O_3 profiles from a number of tropical stations. These sonde measurements have been operating under the Southern Hemisphere Additional Ozonesondes (SHADOZ) (web site http://code916.gsfc.nasa.gov./Data_services/Data.html). Shown is a linear fit $\Omega_{0-5km} = \beta\Omega_{TCO}$ to the data which indicates a slope $\beta = 0.43 \pm 0.013(2\sigma)$. Hence on average when TCO changes by +1 DU, 0-5 km column O_3 changes by around +0.43 DU.

The TOMS algorithm assumes around 15 DU for 0-5 km column O_3 in the tropics. A first order efficiency correction ($\Delta\Omega_{TCO}$) for initially measured CCD TCO (Ω_{TCO}) is given by $\Delta\Omega_{TCO} = \epsilon[\beta\Omega_{TCO} - 15]$ where β is the slope in Figure 12 and ϵ is a retrieval efficiency parameter for TOMS 0-5 km column O_3. However, Ω_{TCO} is presumably not correct as measured by the CCD method so to first order we derive a new value for Ω_{TCO} by $\Omega_{TCO} \rightarrow \Omega_{TCO} + \Delta\Omega_{TCO}$ which yields a new value for Ω_{TCO} given by $[1 + \beta\epsilon]\Omega_{TCO} - 15\epsilon$. Substituting this in the expression for $\Delta\Omega_{TCO}$ yields a final first-order correction for TCO given by $\Delta\Omega_{TCO} = \beta\epsilon[1 + \beta\epsilon]\Omega_{TCO} - 15\beta\epsilon^2 - 15\epsilon$. For altitude range 0-5 km, $\beta = 0.43$ and $\epsilon = 0.5$ and this yields $\Delta\Omega_{TCO} = 0.26\Omega_{TCO} - 9.1$ DU. Note that the correction to Ω_{TCO} is zero for $\Omega_{TCO} = 35$ DU (i.e., $9.1/0.26 = 35$ DU). Adjustments for monthly CCD data were found to be on average (in climatology) at most about 2 to 3 DU (around +2 to +3 DU adjustment in the Atlantic and -2 to -3 DU adjustment over the Pacific).

Acknowledgments. We wish to thank Anne Thompson for expertise with managing the SHADOZ project and the many individuals involved in it including Sam Oltmans and Frank Schmidlin, and also Jacquelyn Witte for providing all of the SHADOZ data in an easy to incorporate format.

References

Chandra, S., J. R. Ziemke, W. Min, and W. G. Read, Effects of 1997-1998 El Niño on tropospheric ozone and water vapor, *Geophys. Res. Lett., 25*, 3867–3870, 1998.

Eck, T. F., P. K. Bhartia, P. H. Hwang, and L. L. Stowe, Reflectivity of Earth's surface and clouds in ultraviolet from satellite observations, *J. Geophys. Res., 92*, 4287–4296, 1987.

Fishman, J., C. E. Watson, J. C. Larsen, and J. A. Logan, Distribution of tropospheric ozone determined from satellite data, *J. Geophys. Res., 95*, 3599–3617, 1990.

Fishman, J., V. G. Brackett, E. V. Browell, and W. B. Grant, Tropospheric ozone derived from TOMS/SBUV measurements during TRACE A, *J. Geophys. Res., 101*, 24,069–24,082, 1996.

Fishman, J., and A. E. Balok, Calculation of daily tropospheric ozone residuals using TOMS and empirically improved SBUV measurements: Application to an ozone pollution episode over the eastern United States, *J. Geophys. Res., 104*, 30,319-30,340, 1999.

Hudson, R. D., J.-H. Kim, and A. M. Thompson, On the derivation of tropospheric column ozone from radiances measured by the total ozone mapping spectrometer, *J. Geophys. Res., 100*, 11,137–11,145, 1995.

Hudson, R. D., and A. M. Thompson, Tropical tropospheric ozone (TTO) from TOMS by a modified-residual method, *J. Geophys. Res. 103*, 22,129–22,145, 1998.

Joiner, J., P. K. Bhartia, R. P. Cebula, E. Hilsenrath, R. D. McPeters, and H. Park, Rotational Raman scattering (Ring effect) in satellite backscatter ultraviolet measurements, *Appl. Optics, 34*, 4513-4525, 1995.

Joiner, J., and P. K. Bhartia, The determination of cloud pressures from rotational Raman scattering in satellite backscatter ultraviolet measurements, *J. Geophys. Res., 100*, 23,019-23,026, 1995.

Klenk, K. F., P. K. Bhartia, A. J. Fleig, V. G. Kaveeshwar, R. D. Mcpeters, P. M. Smith, Total ozone determination from the backscattered ultraviolet (BUV) experiment *J. Appl. Meteorol., 21*, 1672-1684, 1982.

Stowe, L. L., et al., Nimbus-7 global cloud climatology. Part I: Algorithms and validation, *J.*

Clim., *1*, 445–470, 1988.

Stowe, L. L., et al., Nimbus-7 global cloud climatology. Part II: First year results, *J. Clim.*, *2*, 671–709, 1989.

Thompson, A. M., and R. D. Hudson, Tropical tropospheric ozone (TTO) maps from Nimbus 7 and Earth Probe TOMS by the modified-residual method: Evaluation with sondes, ENSO signals, and trends from Atlantic regional time series, *J. Geophys. Res. Lett.*, *104*, 26,961-26,975, 1999.

Torres, O., and P. K. Bhartia, Impact of tropospheric aerosol absorption on ozone retrieval from BUV measurements, 1999: *J. Geophys. Res.*, *104*, 21,569-21,577, 1999.

Vukovich, F. M., V. Brackett, J. Fishman, and J. E. Sickles, II, On the feasibility of using the tropospheric ozone residual (TOR) for non-climatological studies on a quasi-global scale, *J. Geophys. Res.*, *101*, 9093–9105, 1996.

Ziemke, J. R., and S. Chandra, On tropospheric ozone and the tropical wave 1 in total column ozone, *Proc. 18th Quadrenn. Ozone Symp.*, *1*, 447–450, 1998.

Ziemke, J. R., S. Chandra, and P. K. Bhartia, Two new methods for deriving tropospheric column ozone from TOMS measurements: The assimilated UARS MLS / HALOE and convective-cloud differential techniques, *J. Geophys. Res.*, *103*, 22,115–22,127, 1998.

Ziemke, J. R., and S. Chandra, Seasonal and interannual variabilities in tropical tropospheric ozone, *J. Geophys. Res.*, *104*, 21,425–21,442, 1999.

This manuscript was prepared with the AGU LaTeX macros v3.1.

Figure 1. Schematic illustration of cloud slicing for the case of high resolution measurements of above-cloud column ozone and cloud-top pressures. This schematic shows numbers indicating an ozone mixing ratio of 85 ppbv in the upper troposphere which is an amount often found in midlatitudes or in polluted tropical environments.

Figure 2. Schematic illustration of the statistical ensemble approach used in the study with cloud slicing for deriving tropical tropospheric ozone abundances. Co-located measurements of cloud-top pressure and above-cloud column ozone were averaged monthly over broad 5° × 5° regions. The lower part of this figure indicates that when above-cloud column ozone is plotted versus cloud-top pressure for a perfectly well-mixed ideal atmosphere with no net sources or sinks one ideally obtains a straight line, and the slope of this line directly yields a constant ozone VMR.

Figure 3. Average number of co-located footprint measurements per month of TOMS above-cloud column ozone and THIR cloud-top pressure in the 100-400 hPa interval over the 1979-1984 time period.

Figure 4. TOMS above-cloud column ozone (in DU) versus THIR cloud-top pressure (units hPa) scatter plots for the month of February 1981 over the Atlantic (top frames) and western Pacific (bottom frames). Indicated in each frame are line fits for estimating average VMR from cloud slicing. Statistical 2σ values are shown in parentheses.

Figure 5. Seasonal (3-month seasonal averages indicated in each frame) line plots of CCD derived TCO (top curves), 400-1000 hPa column O_3 (middle curves), and 100-400 hPa (bottom curves) at (a) latitude 2.5°N and (b) latitude 2.5°S. The data were derived from a 6-year (1979-1984) climatology. The 400-1000 hPa column O_3 amounts were derived by subtracting 100-400 hPa column O_3 from TCO. Statistical $\pm 2\sigma$ values are shown for all computed quantities.

Figure 6. Top frames: Two nearby time series of CCD derived TCO (top curves) and 100-400 hPa column O_3 from cloud slicing (bottom curves) for a region off the west coast of equatorial Africa. Time series for 100-400 hPa column O_3 were digitally low-pass filtered (shown in bold) with half-frequency response at 5 months. Statistical $\pm 2\sigma$ values for 100-400 hPa column O_3 are shown. For TCO, 2σ is approximately 5 DU. Bottom frames: Climatologies corresponding to the above two time series. Shown are TCO (top curves), 400-1000 hPa column O_3 (middle curves), and 100-400 hPa column O_3 (bottom curves) climatologies. Statistical $\pm 2\sigma$ values are indicated.

Figure 7. Same as Figure 6 but for a region in equatorial western South America.

Figure 8. Twelve-month climatologies corresponding to four nearby regions in the northern part of South America. Shown are CCD derived TCO (top curves), 400-1000 hPa column O_3 (middle curves), and 100-400 hPa column O_3 (bottom curves) climatologies. Statistical $\pm 2\sigma$ values are indicated.

Figure 9. Same as Figure 8 but for four nearby regions in the western Pacific.

Figure 10. Same as Figure 8 but for four nearby regions in the eastern Pacific.

Figure 11. Natal (5°S, 35°W) ozonesonde (dotted and dashed curves) and cloud slicing column ozone (stars) 1979-1984 climatology amounts centered at grid point 2.5°S, 32.5°W. Also shown is the coincident CCD derived TCO climatology (bold).

Figure 12. Column O_3 for altitude range 0-5 km versus TCO from Southern Hemisphere Additional Ozonesondes (SHADOZ) O_3 data. The number of profiles is 115 involving 8 tropical stations for 1995-1999. Also shown is a linear fit to the data which indicates a slope $0.43 \pm 0.013(2\sigma)$. Correlation r is $+0.98$.

Plate 1. Seasonal (3-month seasonal averages indicated in each frame) 6-year (1979-1984) climatology of 100-400 hPa column O_3 (in DU) derived from cloud slicing. Column O_3 was calculated by regression line fitting of all TOMS above-cloud column O_3 and THIR cloud-top pressure data pairs lying within the 100 hPa to 400 hPa pressure band.

Plate 2. Seasonal (3-month seasonal averages indicated in each frame) 6-year (1979-1984) climatology of CCD derived TCO (in DU).

Plate 3. Seasonal (3-month seasonal averages indicated in each frame) 6-year (1979-1984) climatology of 400-1000 hPa column O_3 (in DU). The data were derived by subtracting 100-400 hPa column amounts (shown in Plate 1) from co-located CCD derived TCO measurements in Plate 2.

Using Cloud Tops To Obtain Mean O3 Volume Mixing Ratio

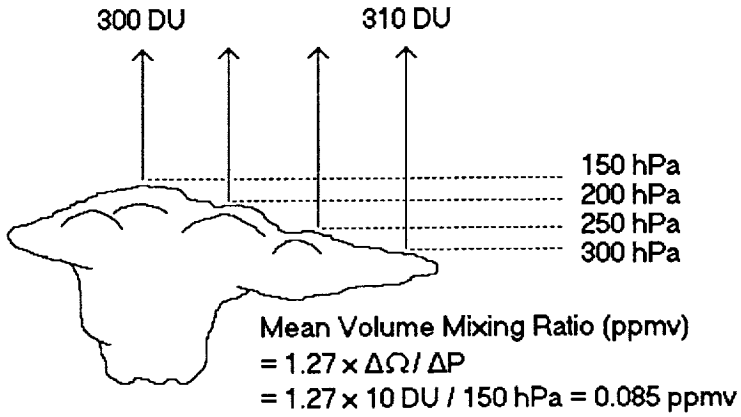

F 1

"ENSEMBLE" CLOUD SLICING

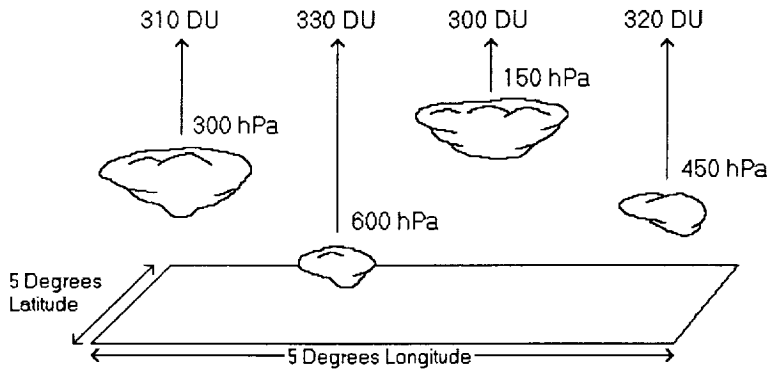

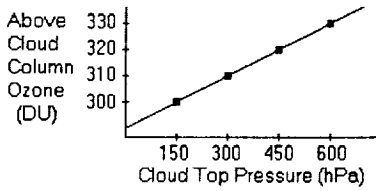

Mean Mixing Ratio (ppmv)
= 1.27 X SLOPE
= 1.27 X (30/450)
= 0.085

F1

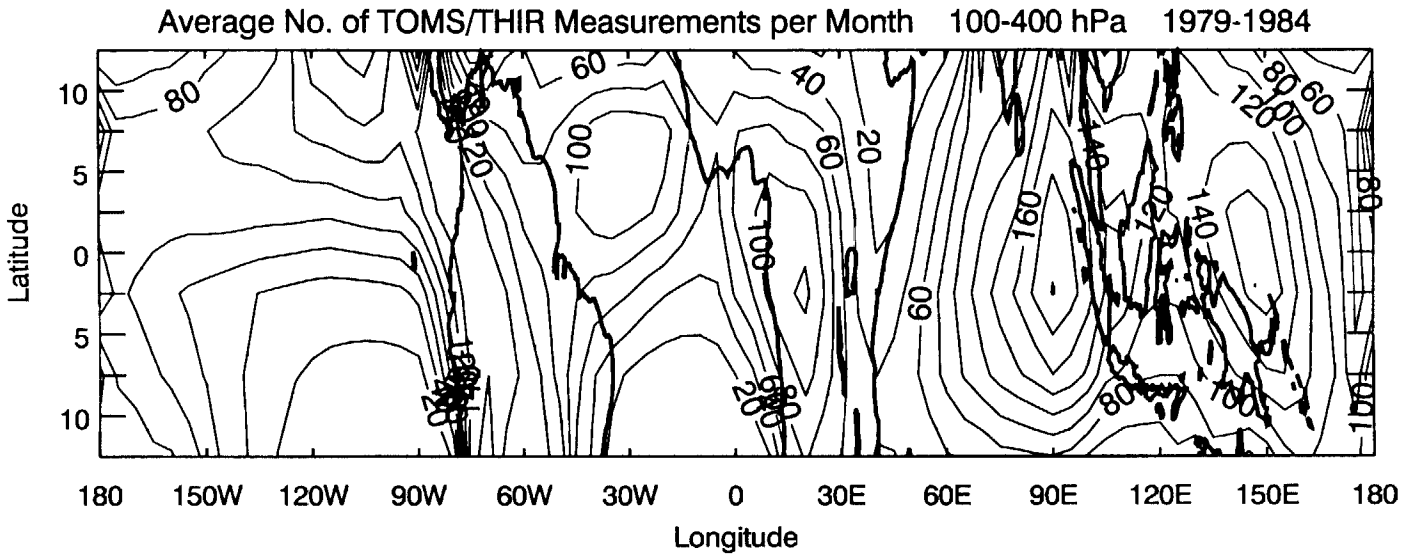
Average No. of TOMS/THIR Measurements per Month 100-400 hPa 1979-1984
Latitude
10
5
0
5
10
180
150W
120W
90W
60W
30W
0
30E
60E
90E
120E
150E
180
Longitude

F3

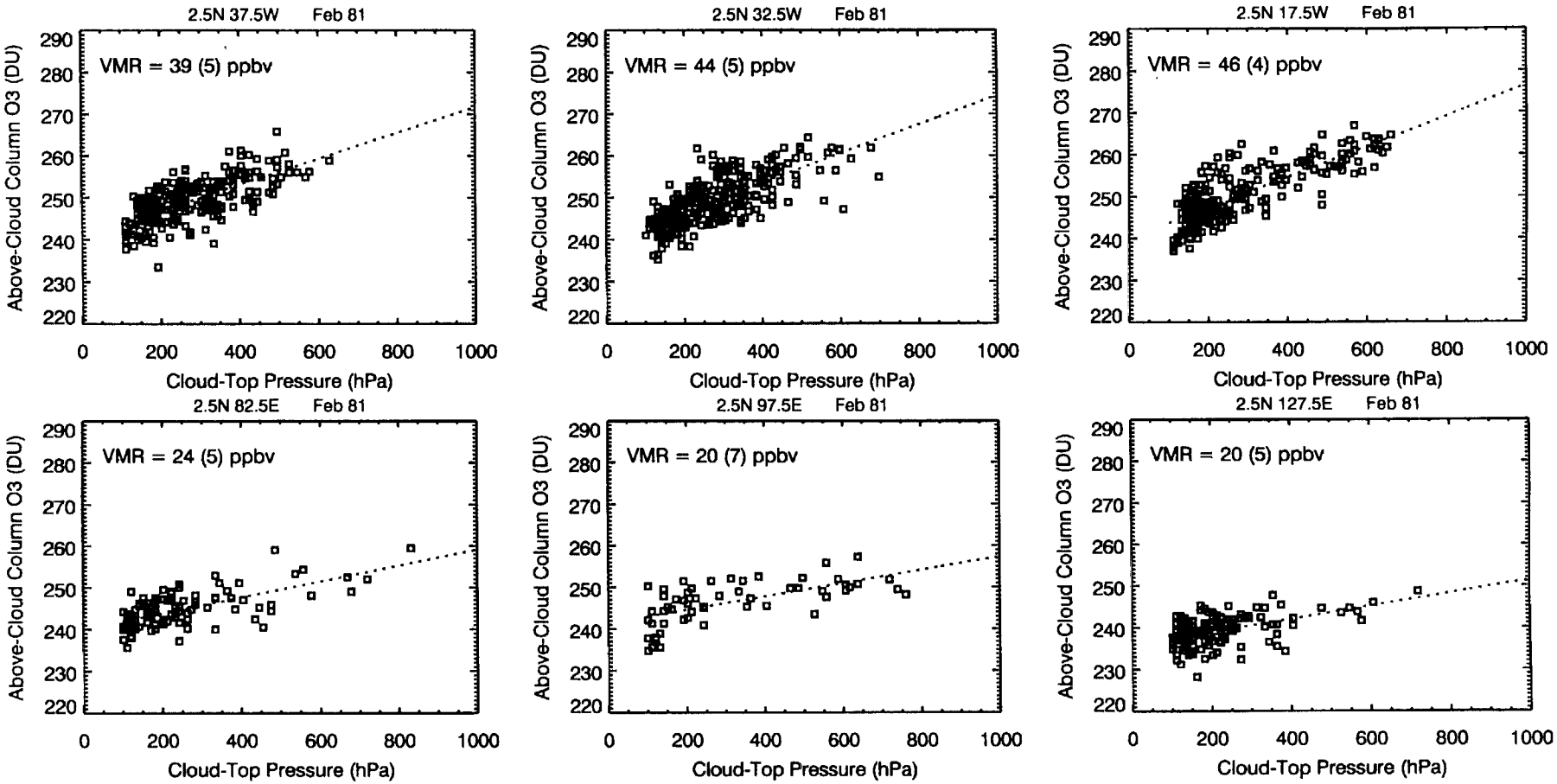
2.5N 37.5W Feb 81
VMR = 39 (5) ppbv
2.5N 32.5W Feb 81
VMR = 44 (5) ppbv
2.5N 17.5W Feb 81
VMR = 46 (4) ppbv
2.5N 82.5E Feb 81
VMR = 24 (5) ppbv
2.5N 97.5E Feb 81
VMR = 20 (7) ppbv
2.5N 127.5E Feb 81
VMR = 20 (5) ppbv
Above-Cloud Column O3 (DU)
Cloud-Top Pressure (hPa)
220
230
240
250
260
270
280
290
0
200
400
600
800
1000

F-4

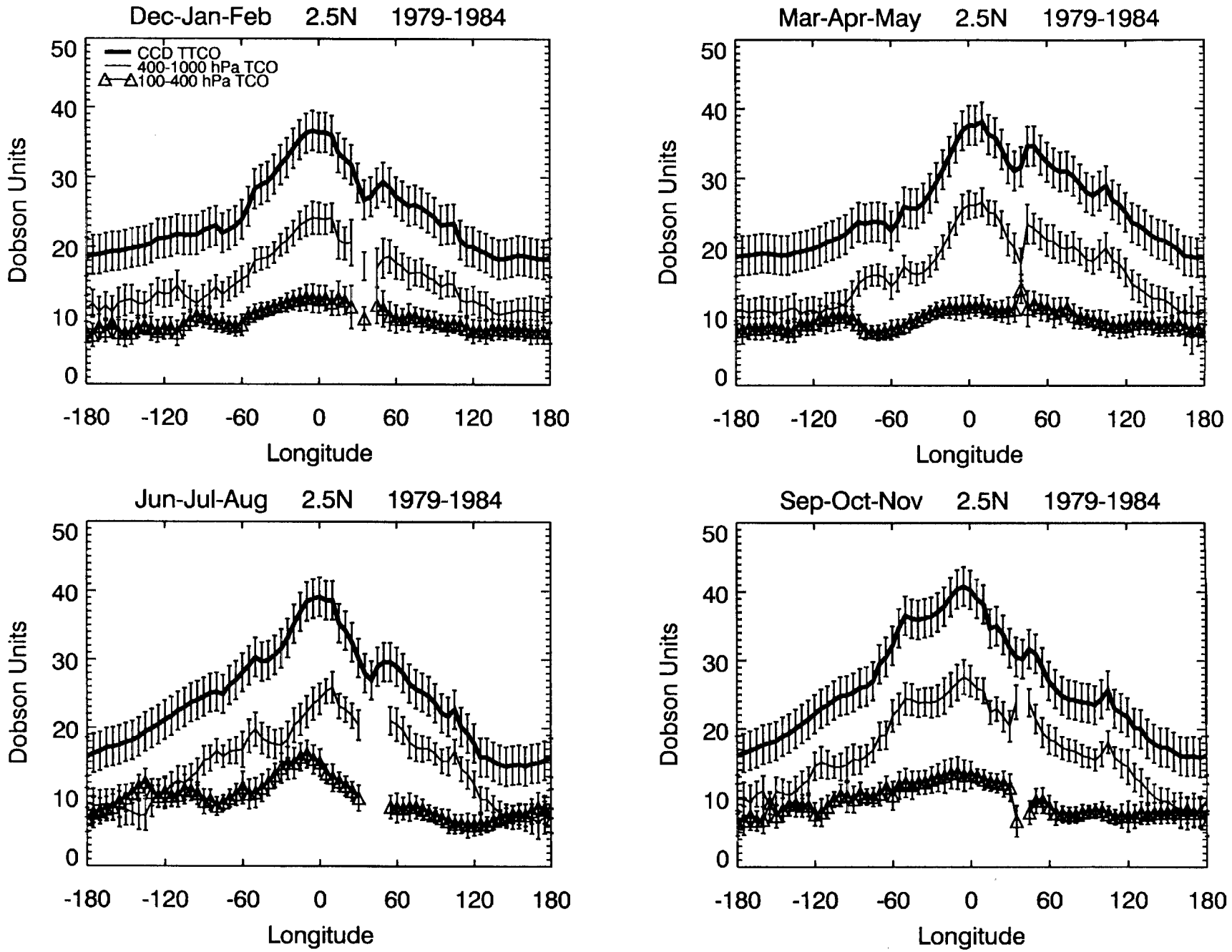
Dec-Jan-Feb 2.5N 1979-1984
CCD TTCO
400-1000 hPa TCO
100-400 hPa TCO
Dobson Units
Longitude
Mar-Apr-May 2.5N 1979-1984
Dobson Units
Longitude
Jun-Jul-Aug 2.5N 1979-1984
Dobson Units
Longitude
Sep-Oct-Nov 2.5N 1979-1984
Dobson Units
Longitude

F5a

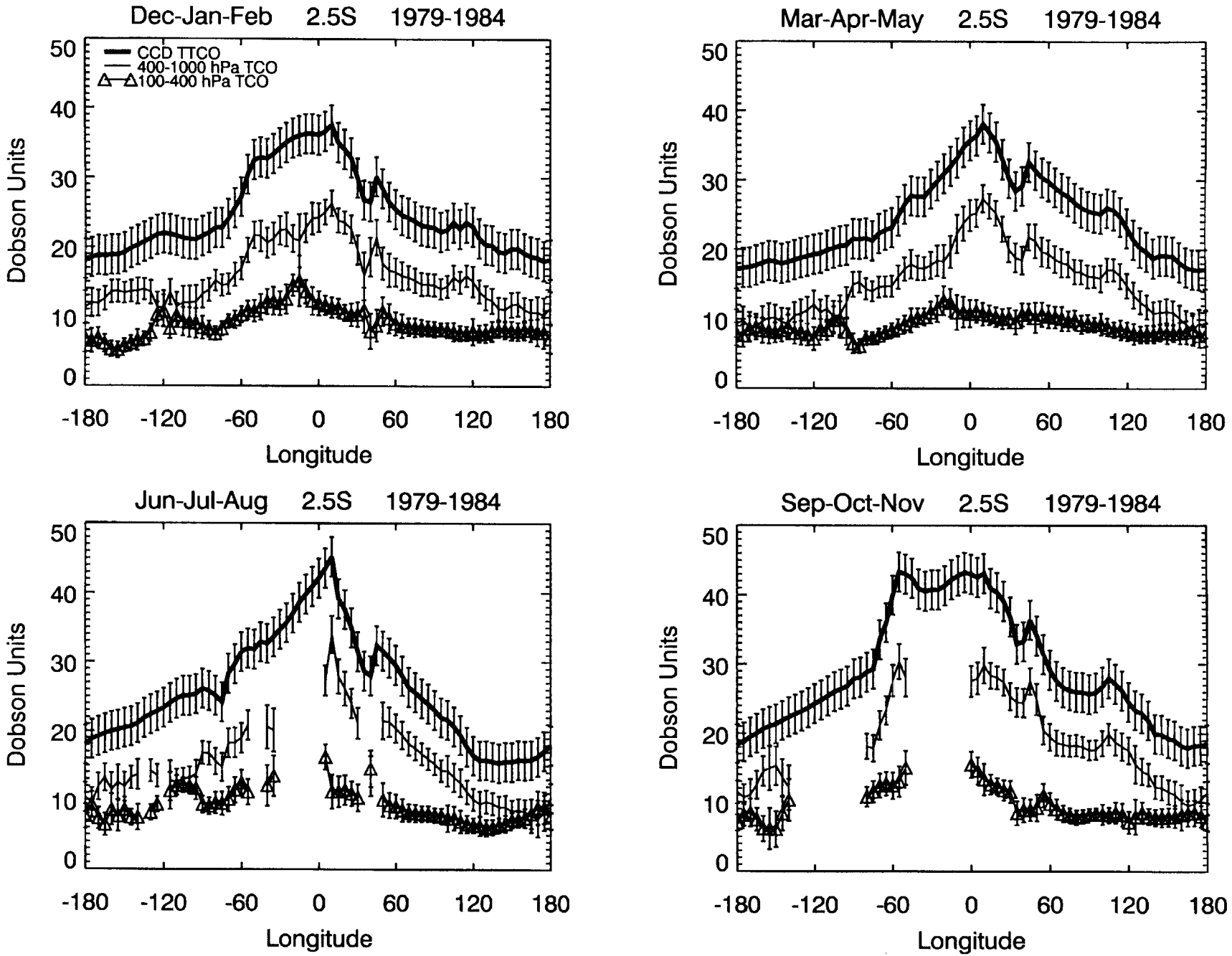
Dec-Jan-Feb 2.5S 1979-1984
CCD TTCO
400-1000 hPa TCO
100-400 hPa TCO
Dobson Units
Longitude
Mar-Apr-May 2.5S 1979-1984
Dobson Units
Longitude
Jun-Jul-Aug 2.5S 1979-1984
Dobson Units
Longitude
Sep-Oct-Nov 2.5S 1979-1984
Dobson Units
Longitude

F5b

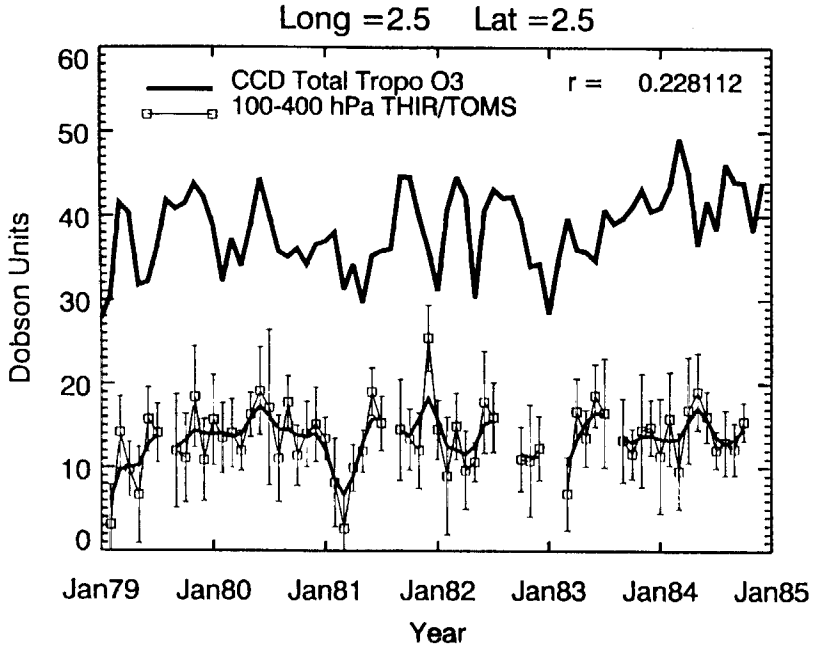
Long =2.5 Lat =2.5
CCD Total Tropo O3
100-400 hPa THIR/TOMS
r = 0.228112
Dobson Units
0
10
20
30
40
50
60
Jan79
Jan80
Jan81
Jan82
Jan83
Jan84
Jan85
Year

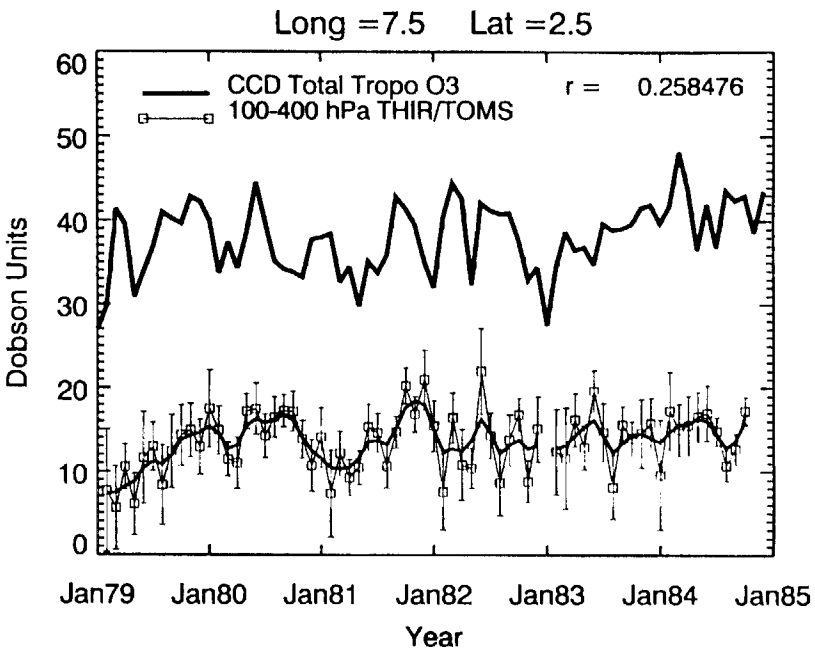
Long =7.5 Lat =2.5
CCD Total Tropo O3
100-400 hPa THIR/TOMS
r = 0.258476
Dobson Units
0
10
20
30
40
50
60
Jan79
Jan80
Jan81
Jan82
Jan83
Jan84
Jan85
Year

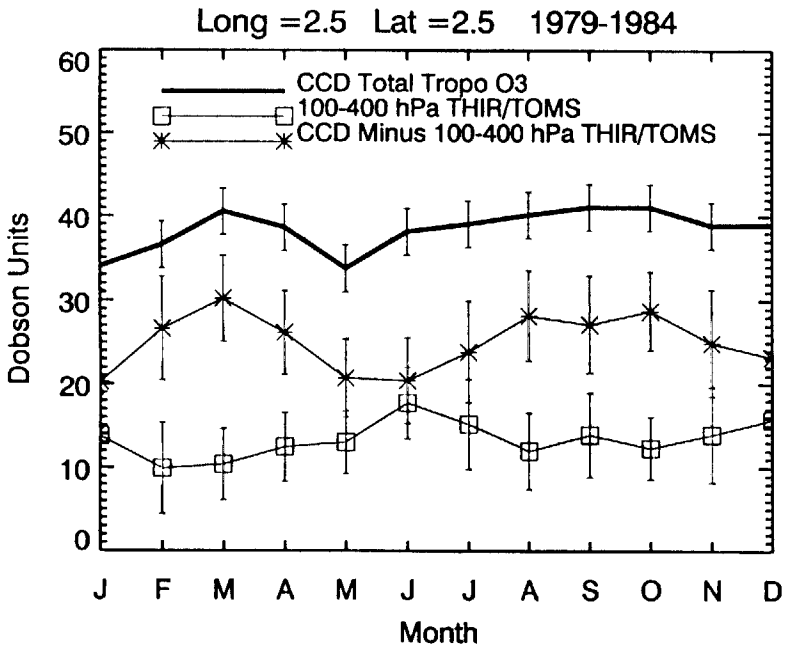
Long =2.5 Lat =2.5 1979-1984
CCD Total Tropo O3
100-400 hPa THIR/TOMS
CCD Minus 100-400 hPa THIR/TOMS
Dobson Units
0
10
20
30
40
50
60
J
F
M
A
M
J
J
A
S
O
N
D
Month

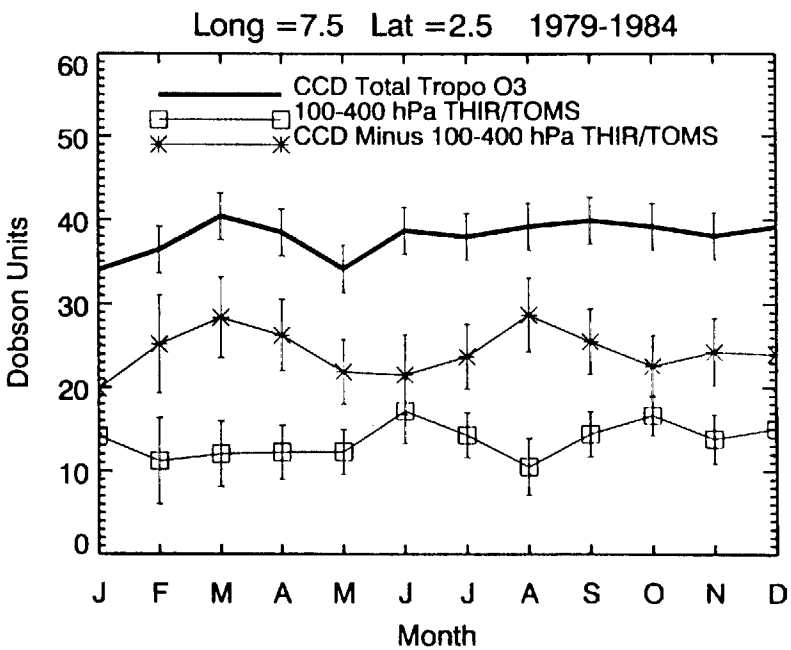
Long =7.5 Lat =2.5 1979-1984
CCD Total Tropo O3
100-400 hPa THIR/TOMS
CCD Minus 100-400 hPa THIR/TOMS
Dobson Units
0
10
20
30
40
50
60
J
F
M
A
M
J
J
A
S
O
N
D
Month

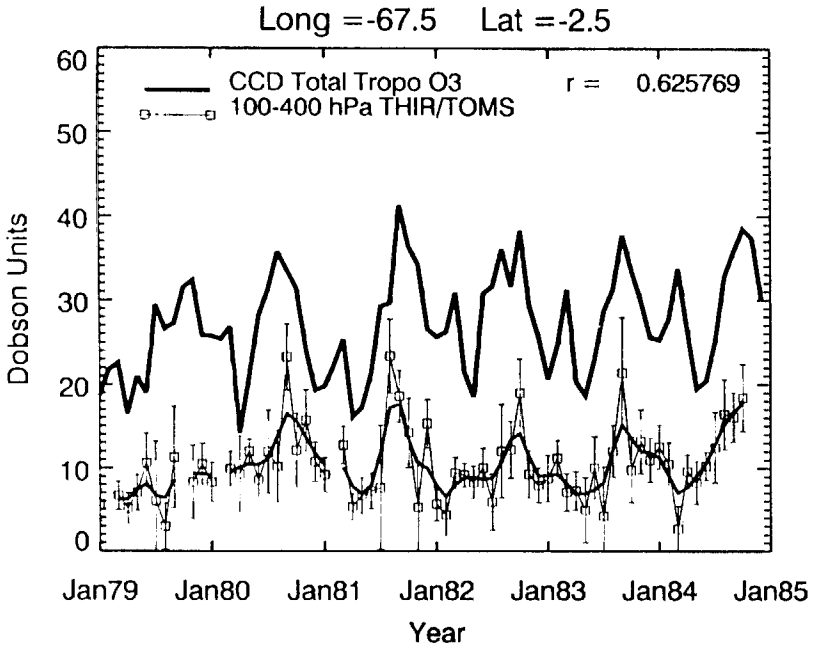
Long =-67.5 Lat =-2.5
CCD Total Tropo O3
100-400 hPa THIR/TOMS
r = 0.625769
Dobson Units
Year
Jan79 Jan80 Jan81 Jan82 Jan83 Jan84 Jan85

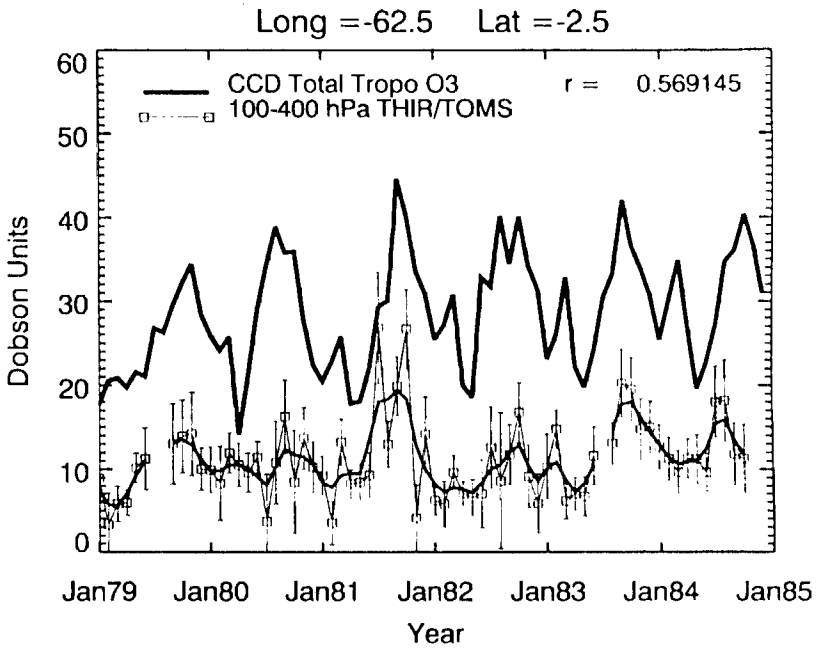
Long =-62.5 Lat =-2.5
CCD Total Tropo O3
100-400 hPa THIR/TOMS
r = 0.569145
Dobson Units
Year
Jan79 Jan80 Jan81 Jan82 Jan83 Jan84 Jan85

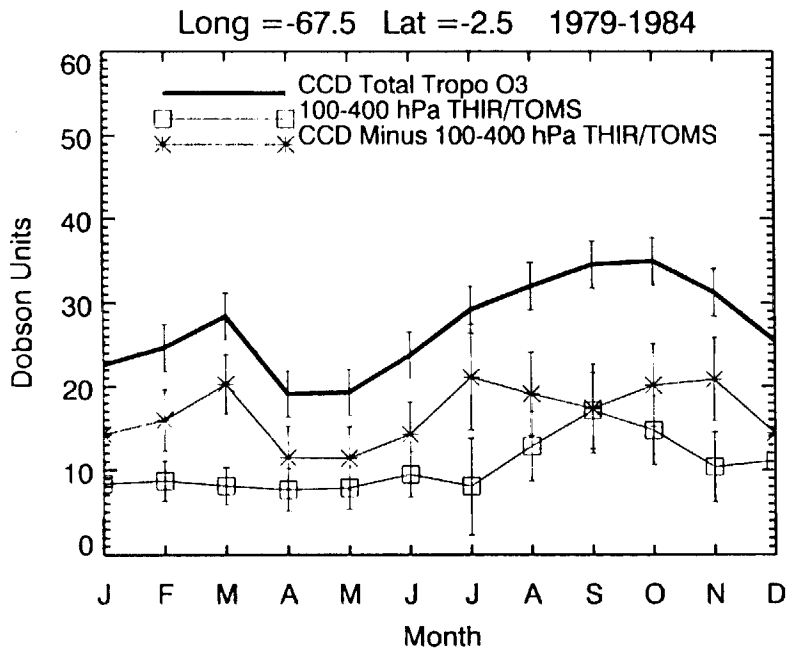
Long =-67.5 Lat =-2.5 1979-1984
CCD Total Tropo O3
100-400 hPa THIR/TOMS
CCD Minus 100-400 hPa THIR/TOMS
Dobson Units
Month
J F M A M J J A S O N D

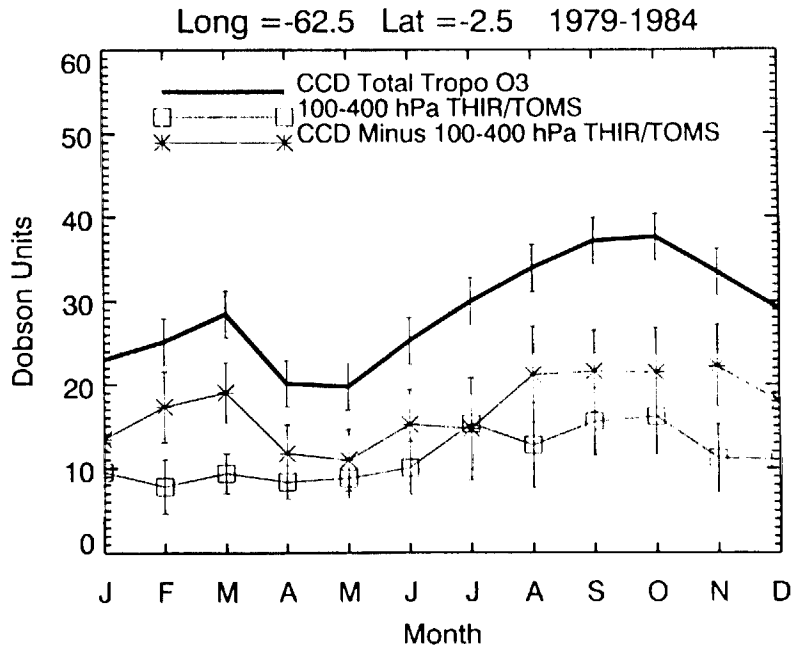
Long =-62.5 Lat =-2.5 1979-1984
CCD Total Tropo O3
100-400 hPa THIR/TOMS
CCD Minus 100-400 hPa THIR/TOMS
Dobson Units
Month
J F M A M J J A S O N D

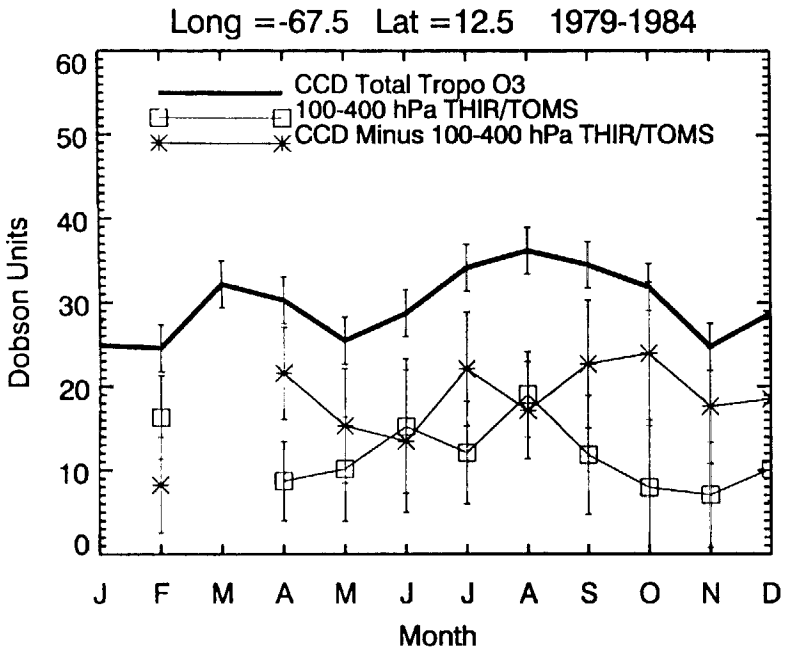
Long =-67.5 Lat =12.5 1979-1984
CCD Total Tropo O3
100-400 hPa THIR/TOMS
CCD Minus 100-400 hPa THIR/TOMS
Dobson Units
Month
J F M A M J J A S O N D

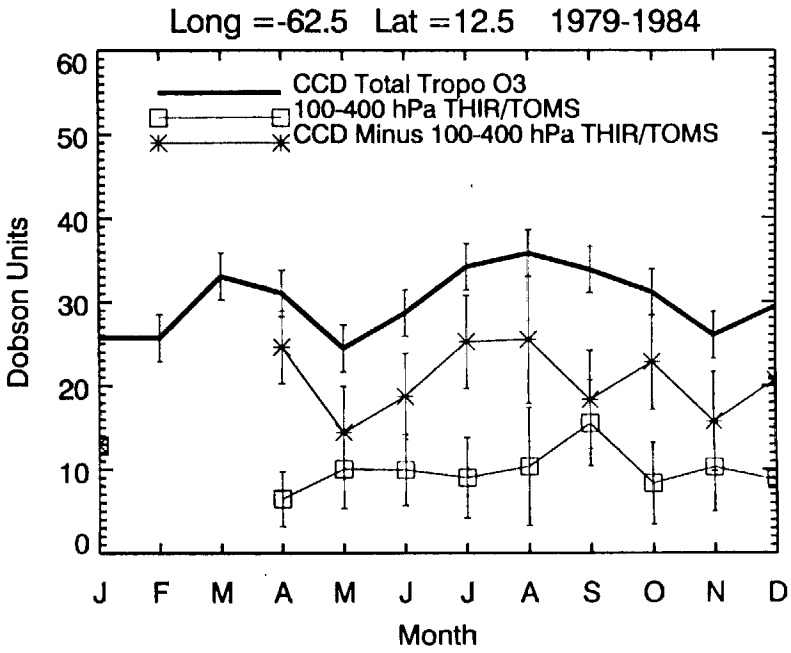
Long =-62.5 Lat =12.5 1979-1984
CCD Total Tropo O3
100-400 hPa THIR/TOMS
CCD Minus 100-400 hPa THIR/TOMS
Dobson Units
Month
J F M A M J J A S O N D

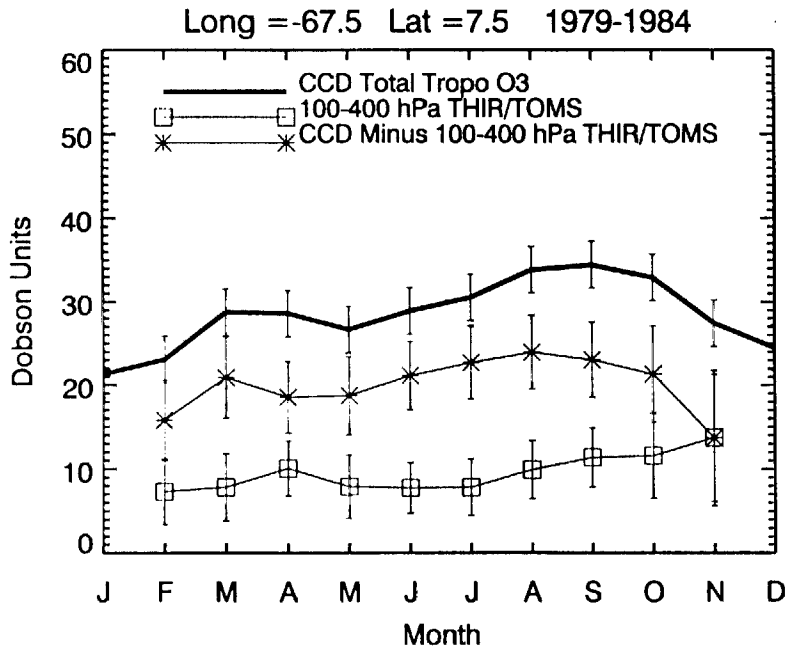
Long =-67.5 Lat =7.5 1979-1984
CCD Total Tropo O3
100-400 hPa THIR/TOMS
CCD Minus 100-400 hPa THIR/TOMS
Dobson Units
Month
J F M A M J J A S O N D

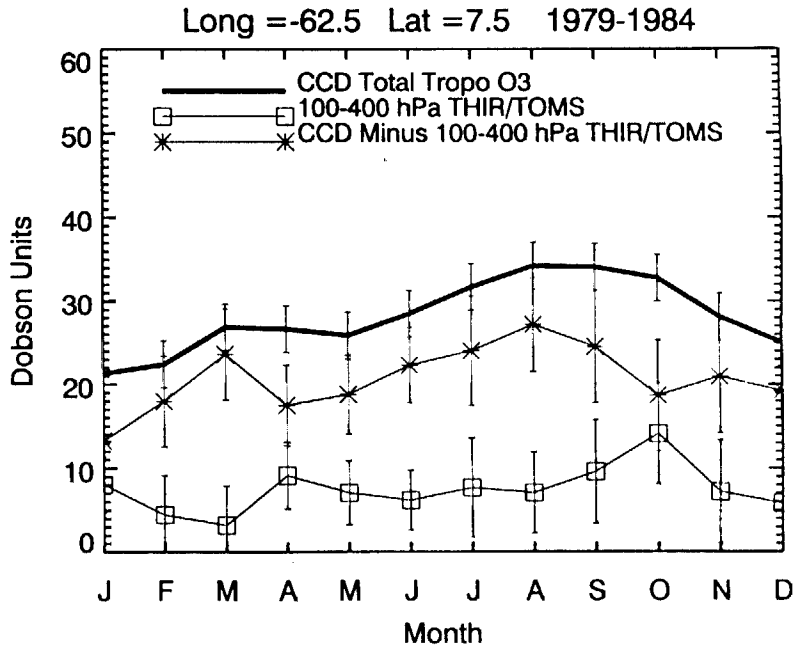
Long =-62.5 Lat =7.5 1979-1984
CCD Total Tropo O3
100-400 hPa THIR/TOMS
CCD Minus 100-400 hPa THIR/TOMS
Dobson Units
Month
J F M A M J J A S O N D

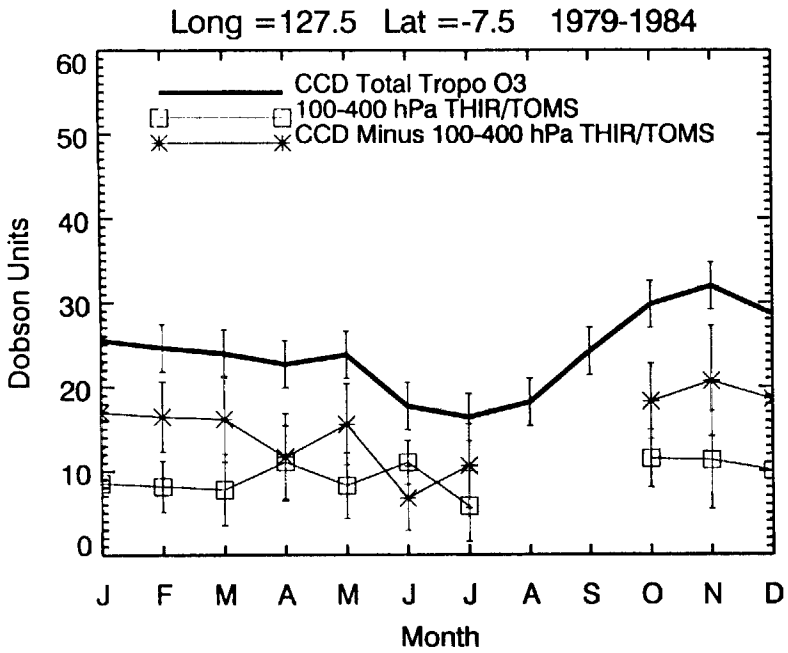
Long =127.5 Lat =-7.5 1979-1984
CCD Total Tropo O3
100-400 hPa THIR/TOMS
CCD Minus 100-400 hPa THIR/TOMS
Dobson Units
Month
J F M A M J J A S O N D

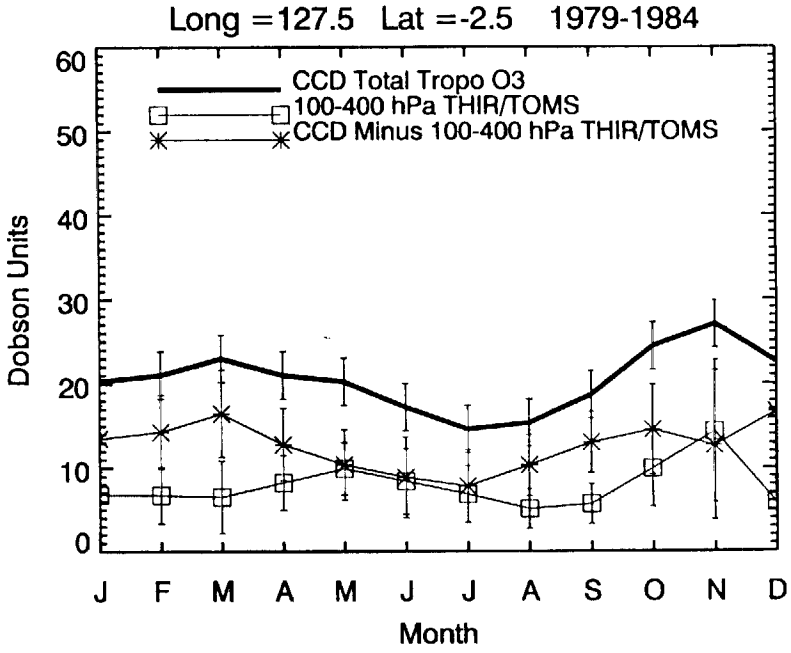
Long =127.5 Lat =-2.5 1979-1984
CCD Total Tropo O3
100-400 hPa THIR/TOMS
CCD Minus 100-400 hPa THIR/TOMS
Dobson Units
Month
J F M A M J J A S O N D

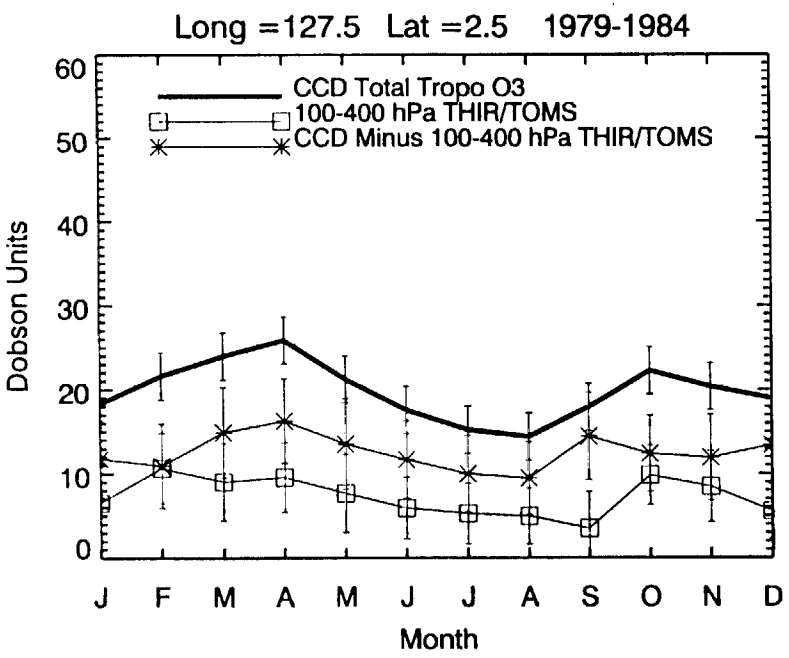
Long =127.5 Lat =2.5 1979-1984
CCD Total Tropo O3
100-400 hPa THIR/TOMS
CCD Minus 100-400 hPa THIR/TOMS
Dobson Units
Month
J F M A M J J A S O N D

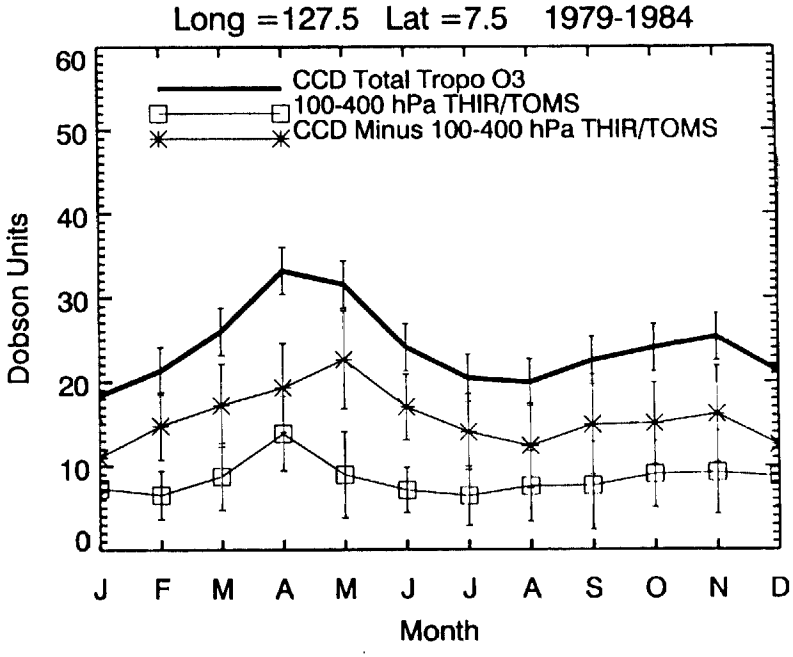
Long =127.5 Lat =7.5 1979-1984
CCD Total Tropo O3
100-400 hPa THIR/TOMS
CCD Minus 100-400 hPa THIR/TOMS
Dobson Units
Month
J F M A M J J A S O N D

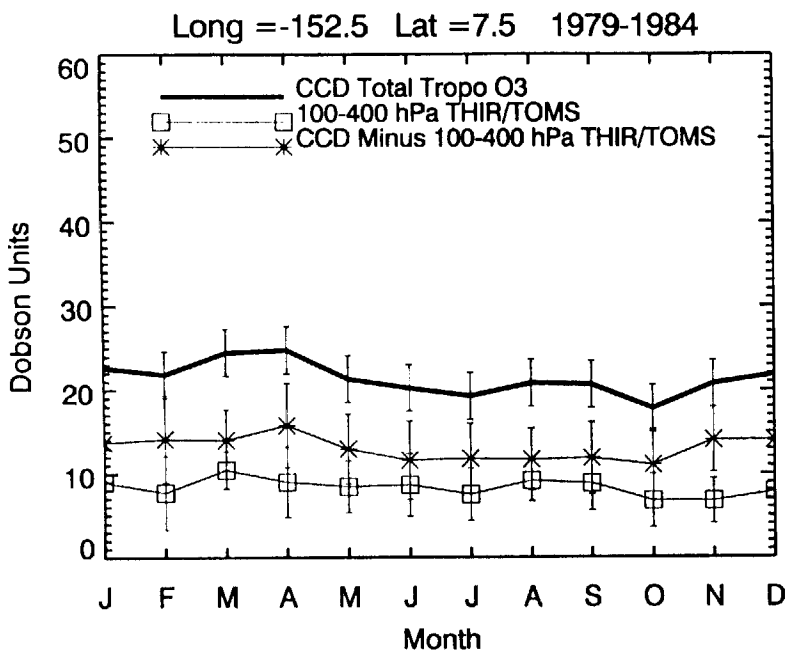
Long =-152.5 Lat =7.5 1979-1984
CCD Total Tropo O3
100-400 hPa THIR/TOMS
CCD Minus 100-400 hPa THIR/TOMS
Dobson Units
Month
J F M A M J J A S O N D

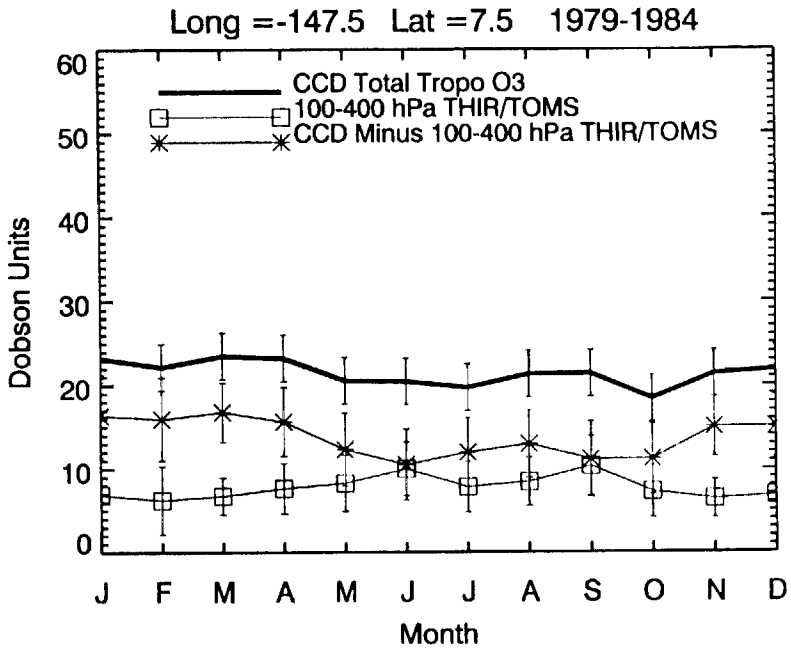
Long =-147.5 Lat =7.5 1979-1984
CCD Total Tropo O3
100-400 hPa THIR/TOMS
CCD Minus 100-400 hPa THIR/TOMS
Dobson Units
Month
J F M A M J J A S O N D

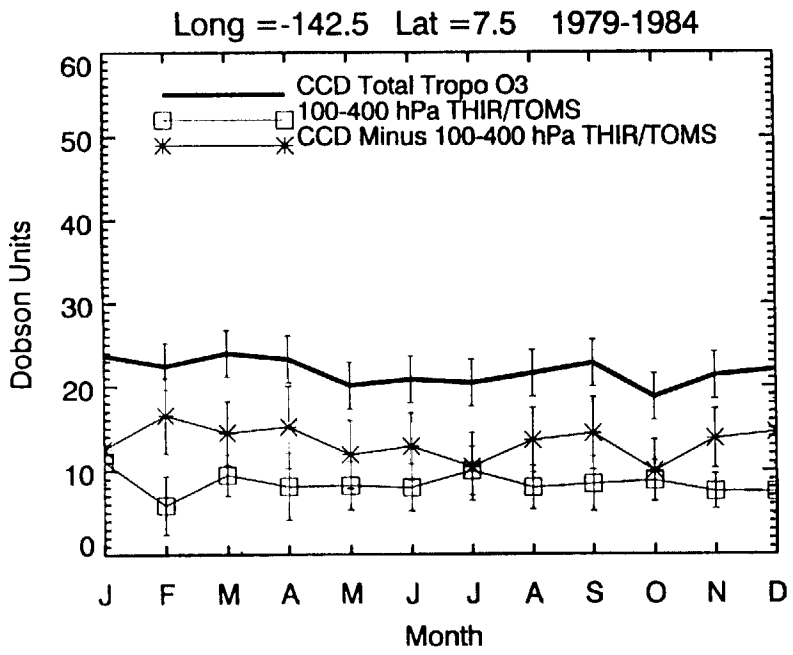
Long =-142.5 Lat =7.5 1979-1984
CCD Total Tropo O3
100-400 hPa THIR/TOMS
CCD Minus 100-400 hPa THIR/TOMS
Dobson Units
Month
J F M A M J J A S O N D

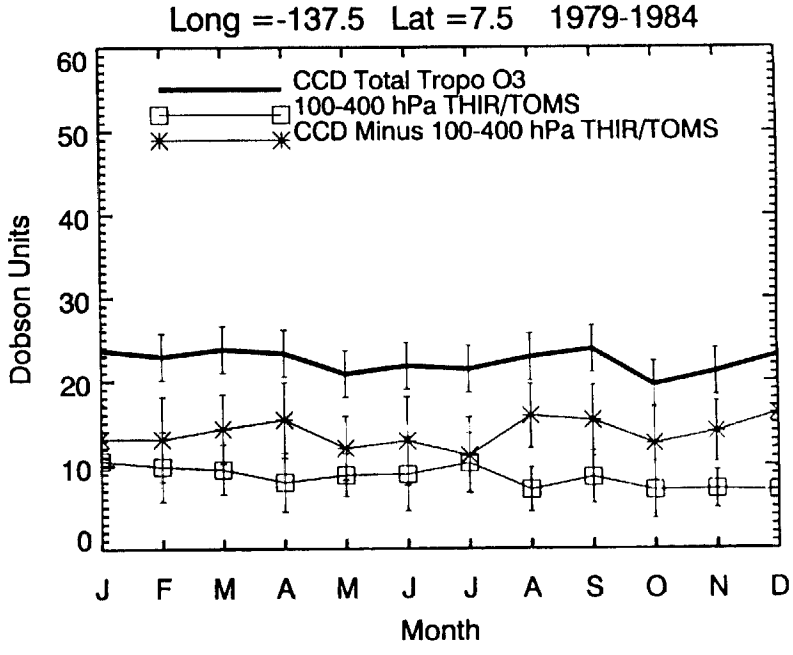
Long =-137.5 Lat =7.5 1979-1984
CCD Total Tropo O3
100-400 hPa THIR/TOMS
CCD Minus 100-400 hPa THIR/TOMS
Dobson Units
Month
J F M A M J J A S O N D

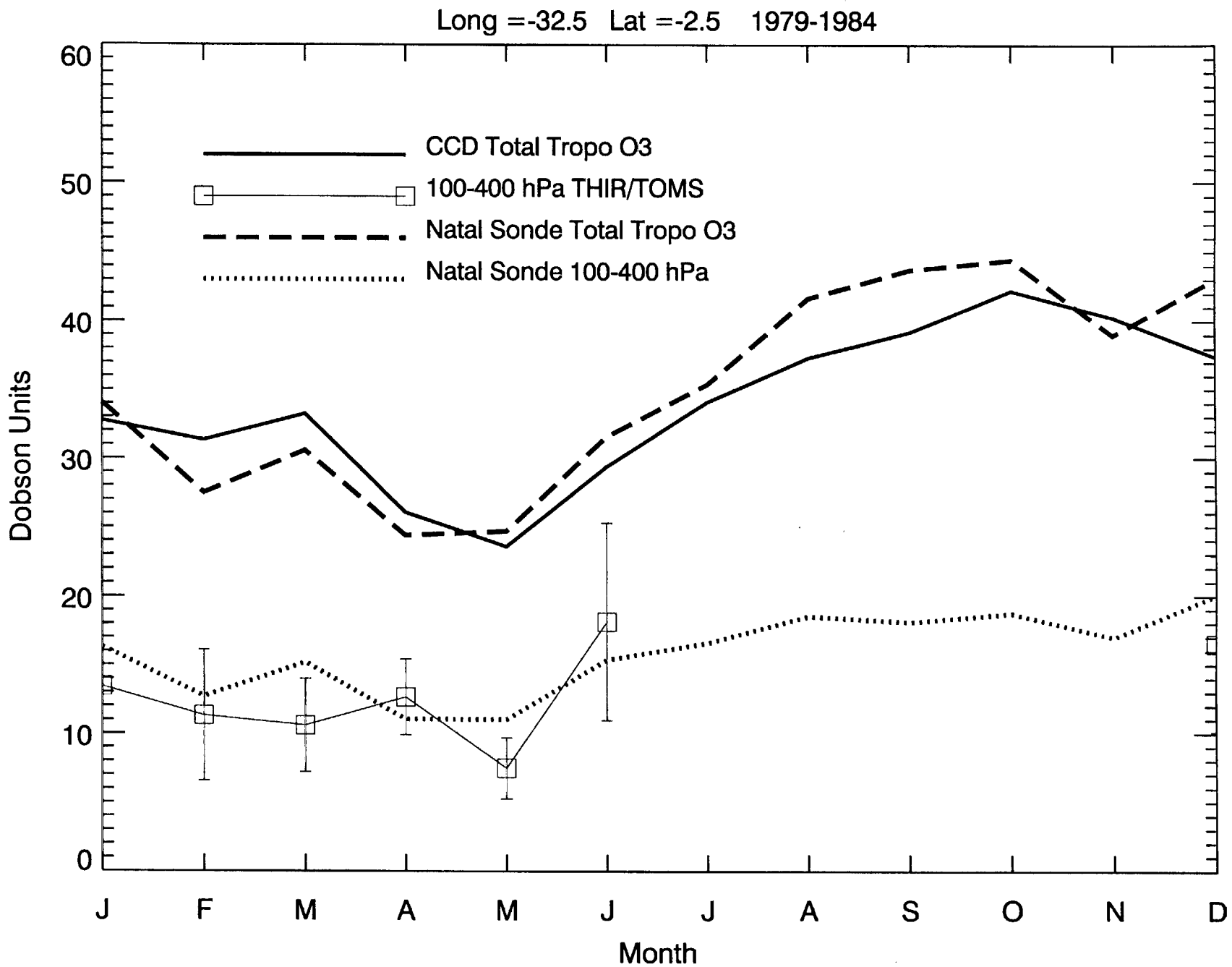
Long =-32.5 Lat =-2.5 1979-1984
CCD Total Tropo O3
100-400 hPa THIR/TOMS
Natal Sonde Total Tropo O3
Natal Sonde 100-400 hPa
Dobson Units
0
10
20
30
40
50
60
J
F
M
A
M
J
J
A
S
O
N
D
Month

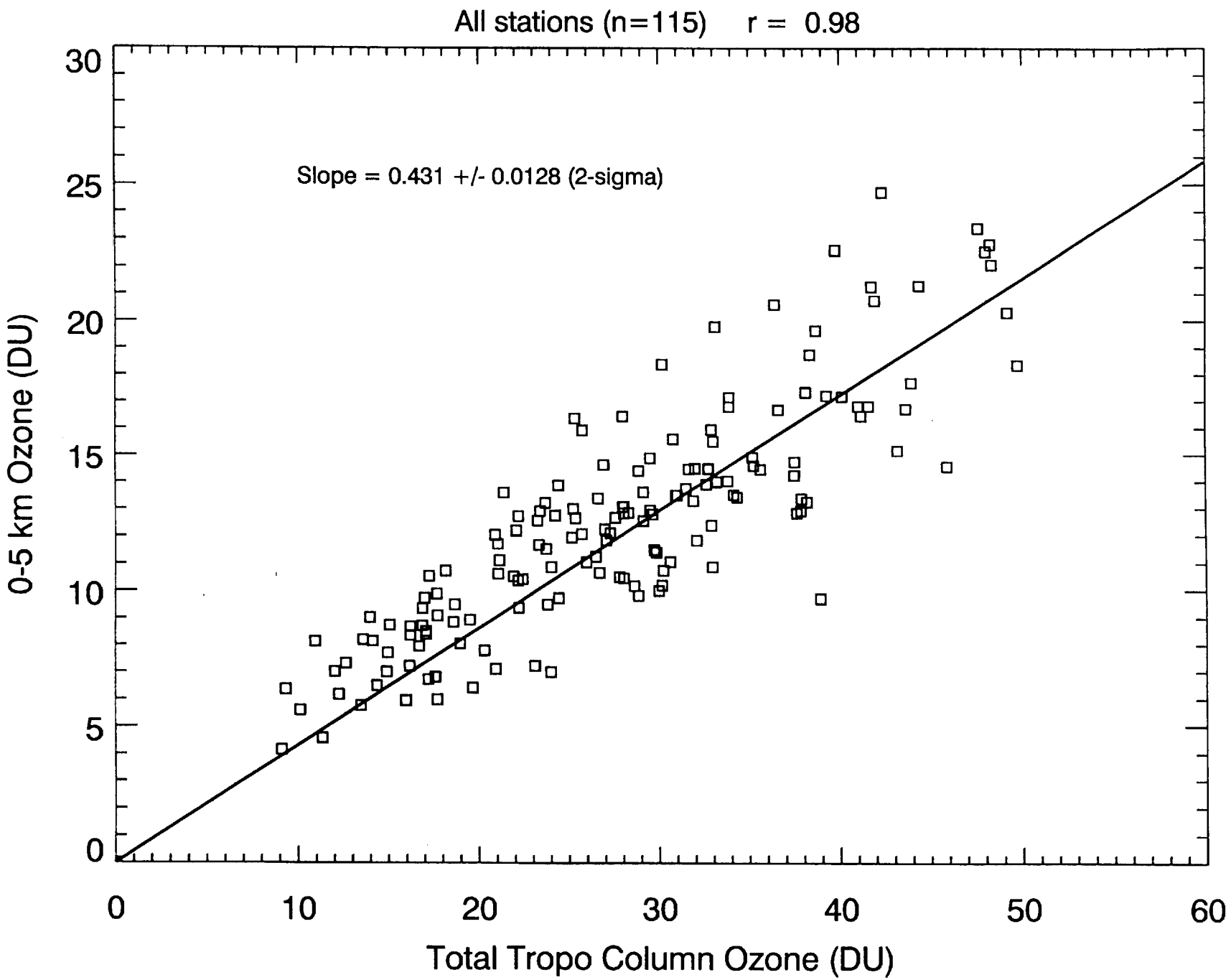
All stations (n=115) r = 0.98
Slope = 0.431 +/- 0.0128 (2-sigma)
0-5 km Ozone (DU)
Total Tropo Column Ozone (DU)
0
5
10
15
20
25
30
0
10
20
30
40
50
60

F17

100-400 hPa TROPOSPHERIC OZONE (DOBSON UNITS)

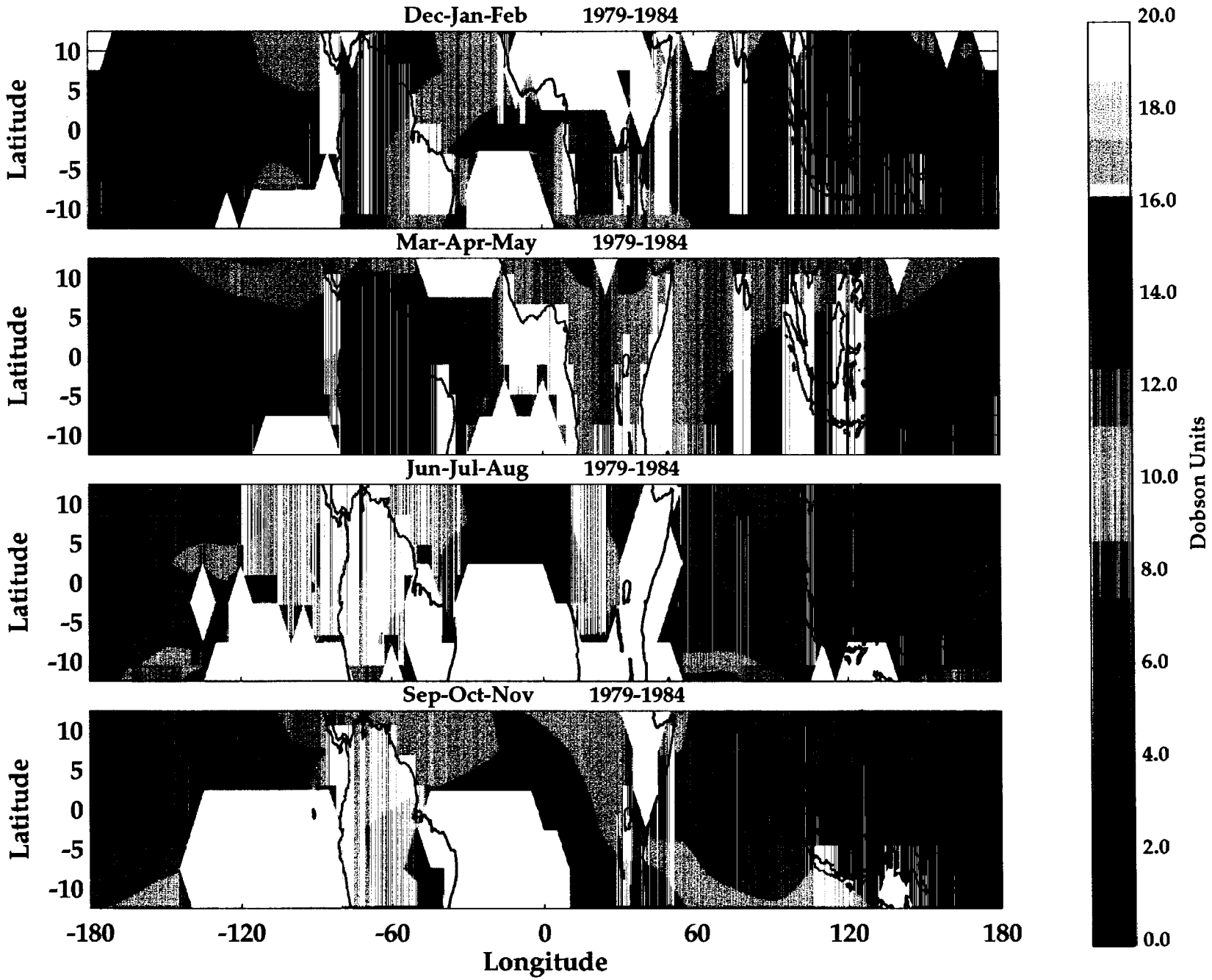

Plate 1

CCD TOTAL TROPOSPHERIC OZONE (DOBSON UNITS)

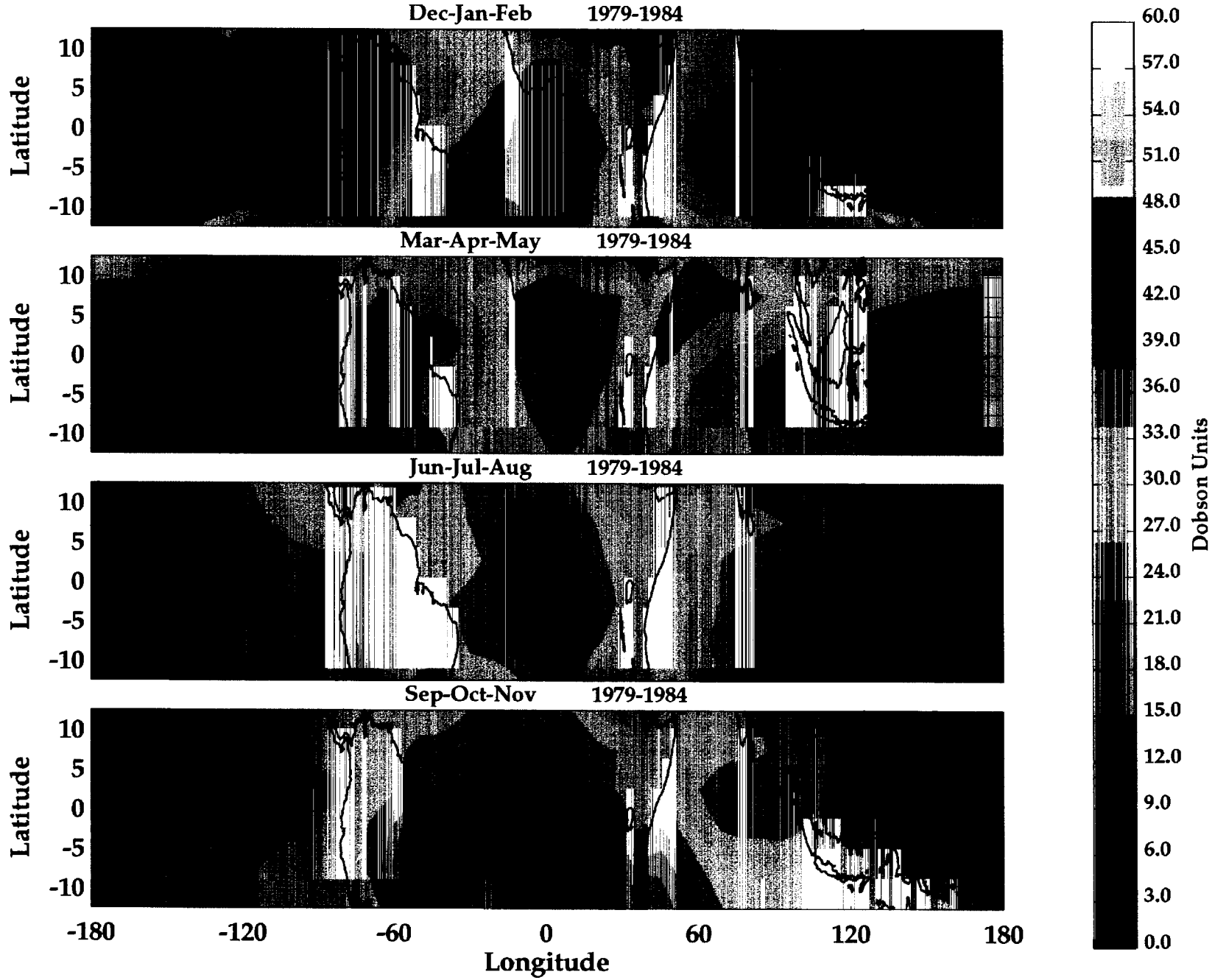

page 2

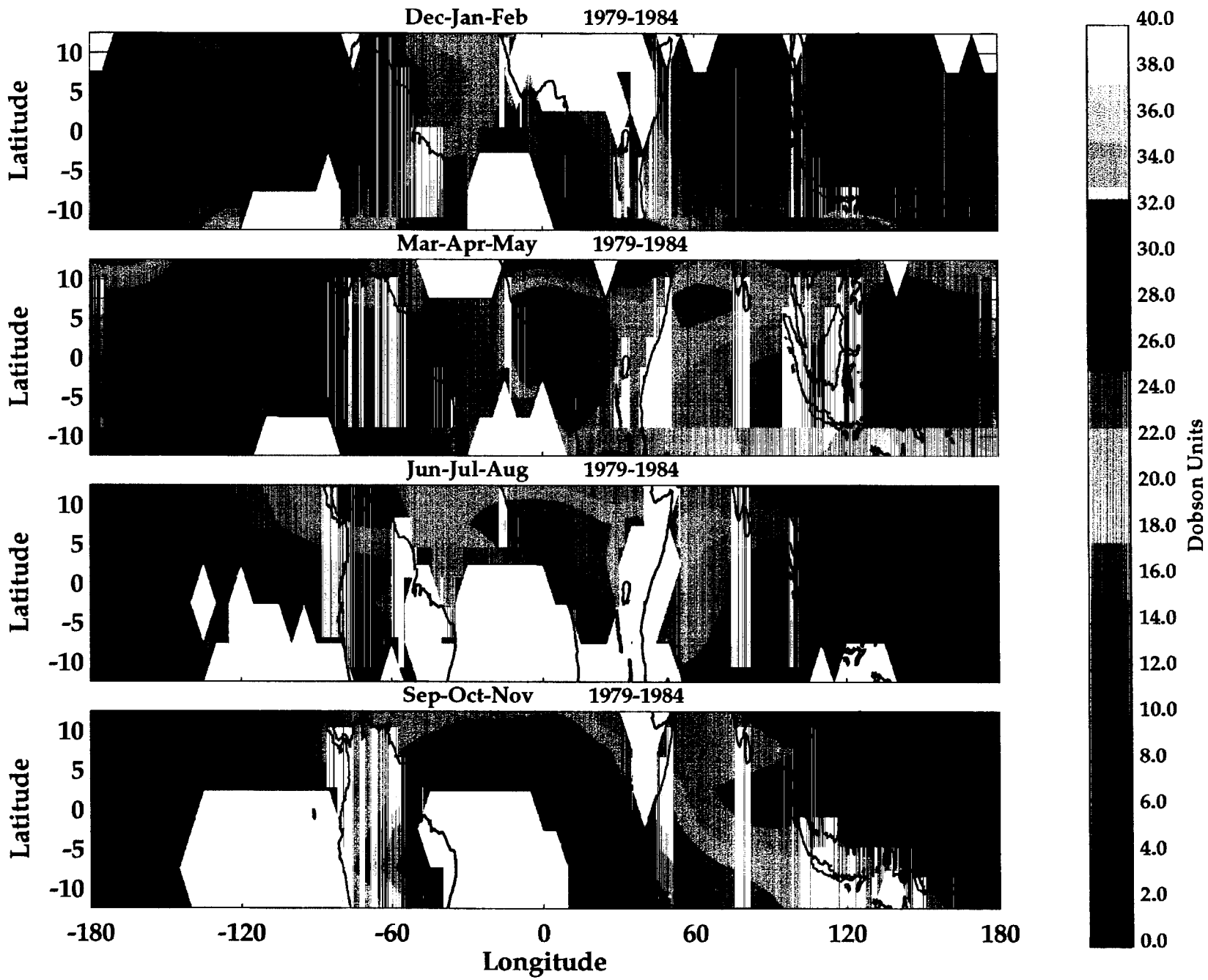
400-1000 hPa TROPOSPHERIC OZONE (DOBSON UNITS)
Dec-Jan-Feb 1979-1984
Mar-Apr-May 1979-1984
Jun-Jul-Aug 1979-1984
Sep-Oct-Nov 1979-1984
Latitude
10
5
0
-5
-10
-180
-120
-60
0
60
120
180
Longitude
40.0
38.0
36.0
34.0
32.0
30.0
28.0
26.0
24.0
22.0
20.0
18.0
16.0
14.0
12.0
10.0
8.0
6.0
4.0
2.0
0.0
Dobson Units

Plate 3